西北工业大学

本科毕业设计论文

题 目 **基于 RANS 和二维稳定性理论的流场分析**

专业名称 飞行器动力工程

学生姓名 李嵩瑞

指导教师 吕亚国、Eusebio Valero

毕业时间 2019 年 7 月 1 日

UNIVERSIDAD POLITÉCNICA DE MADRID

BACHELOR THESIS

Flow Field Analysis Based on RANS Solver and BiGlobal Stability Theory

Author:
Songrui LI

Supervisors:
Prof. Eusebio VALERO
Vice Prof. Yaguo LYU

A thesis submitted in fulfillment of the requirements for the degree of Bachelor

in the

Methods and Numerical Applications to Aerospace Technology
Escuela Técnica Superior de Ingeniería Aeronáutica y del Espacio

June 9, 2019

Declaration of Authorship

I, Songrui LI, declare that this thesis titled, "Flow Field Analysis Based on RANS Solver and BiGlobal Stability Theory" and the work presented in it are my own. I confirm that:

- This work was done wholly or mainly while in candidature for a research degree at this University.
- Where any part of this thesis has previously been submitted for a degree or any other qualification at this University or any other institution, this has been clearly stated.
- Where I have consulted the published work of others, this is always clearly attributed.
- Where I have quoted from the work of others, the source is always given. With the exception of such quotations, this thesis is entirely my own work.
- I have acknowledged all main sources of help.
- Where the thesis is based on work done by myself jointly with others, I have made clear exactly what was done by others and what I have contributed myself.

Signed: _____

Date: _____

UNIVERSIDAD POLITÉCNICA DE MADRID

Abstract

Escuela Técnica Superior de Ingeniería Aeronáutica y del Espacio

Bachelor

Flow Field Analysis Based on RANS Solver and BiGlobal Stability Theory

by Songrui LI

The flow instability inside the jet engines affects the working range, safety and lifespan of the aircraft, and has therefore been one of the focuses of engine design and optimisation. Flow separation and base bleed are two iconic flow instability phenomenon in engines' blades rolls. Aiming at these two problems, this paper combines the Rans equation solver TAU and the BiGloble stability analysis theory to visualise the flow instability and extract the main model of it.

Firstly, a validation case of cylinder flow at $Re = 60$ is simulated and the results of the Strouhal number match the experience data. The main model is extracted as well.

Secondly, a NACA0012 airfoil is studied in a similar method. A set of simulations are performed under a range of angle of attack from 0 to 19 degrees. The critical angle of separation is identified as 18.9 degrees. And the flow topology at 4 angle of attacks is visualised, the main model of the flow at critical angle of attack is also extracted.

Thirdly, a transonic injector case is simulated. Solutions for two kinds of injectors, with straight and rounded trailing edge respectively, are compared with each other. Bifurcation of the bleeding jet-flow and shock waves appear at both cases. While stability analysis failed to performed for certain reasons.

KEYWORDS: RANS equation, stability analysis, NACA0012, jet flow

Contents

Chapter 1

Introduction

1.1 Flow unsteadiness

Unsteady flow is a significant problem that has been studied for years in the field of air propulsion. Dangerous phenomena such as stall and surge would occur and lead to in-air crash and failure if the jet engine operates under harsh conditions. In addition, non-fatal unsteady flow conditions also have a direct adverse effect on engine performance such as efficiency, reliability, and lifespan. To avoid abnormal airflow, it is significant to identify the mechanisms causing such unsteadiness. For example, in aircraft design, it is important to detect the wake vortices from the trailing edge of the wing and control the vortex breaking down to increase wing efficiency.

Turbulence is the main problem, among other things, and the most frequently studied.It is characterised by the dissipation of fluid kinetic energy that is transferred to heat. In the year of 1883, Osborne Reynolds [1] recorded the transition from laminar to turbulent flow by examining the behaviour of water flow at different flow rates. From this experiment, the Reynolds number derived by Reynolds is defined as the ratio of the inertial force to the viscous force of the flow. After that, subsequent researches showed that the Reynolds number also represents the ratio of the length scale of the largest eddy to that of the smallest eddy in the system. As the largest eddies always keep the same magnitude, the eddies in the smallest scale, namely the Kolmogorov microscales [2], are corresponding to the Reynolds number and consequently to the viscous dissipations as well. Furthermore, it is possible to calculate the time scale of eddies as follows. For the maximum motion scale eddies, the temporal scale is defined as L/U, with L the length size of the eddy and U the flow velocity. While for eddies of small magnitude, the time scale is related to the viscosity and the dissipation.

As a result, as the Reynolds number increase, the differences of both the length and the temporal scale between the largest and smallest eddies will increase, giving a method to predict the onset of turbulence numerically. Yet in ideal computation, the time step must be set small enough to capture the time scale of the smallest eddies. To simplify the case and save the computational memory resources, an averaged version of the governing equations are introduced and turbulence models are also adopted to providing a simplified description of the turbulence by filtering the low-frequency turbulence and leaving the high-frequency phenomena. As for studies focusing on the low-frequency portion of the flow, stability analysis is often applied to characterise the response of the flow to tiny perturbations.

1.2 Stability analysis

Linear stability theory (LST) has been successfully applied for predicting and analyzing the transition of parallel shear flows [3] [4] from the 1900s. In this method, a tiny distribution is added into a stable solution of a system. If an exponentially increasing model occurs with the evolution of the perturbation, the flow is defined as unstable. Huerre and Monkewitz [5] and Collis et al. [6] classified the flow unsteadiness into 3 types: convective, absolute and global. Convective and absolute instability apply to strictly parallel flows while global unsteadiness refers to non-parallel flows. Global stability analysis was not widely used until Pierrehumbert and Widnall's work [7]. As a review by Theofilis in [8] and [9], global stability analysis was applied to a wide range of areas.

The application of global stability analysis on two-dimensional basic flows is originated from the work of Luijkx and Platten [10]. And Jackson [11], Zebib [12] and Morzynski & Thiele [13] solved the two-dimensional Global instability, namely Biglobal instability, of flow around a cylinder. Gelfgat [14] did the TriGlobal stability analysis on a Rayleigh-Bénard convection problem. As for the analysis of airfoil case, triple decomposition stability analysis was used by Kitsios et al. [15] on a NACA0015 airfoil. They found eigen- models with a temporal frequency equal to the forcing frequency used in the experiments of Tuck and Soria [16]. Besides, they found the most unstable modes at the critical point of separation. Theofilis et al. [17] performed a Modal BiGlobal analysis on a NACA0012 airfoil at a small angle of attack to monitor incompressible flow. A separation mode at leading edge was found accountable for the instability in the wake.

1.3 Motivation

Of the instability phenomena that are considered problematic for the aerospace industry, there are two topics of interest in the field of turbomachinery, particularly in aircraft turbines. They are separation under the high-lift condition and the transonic base bleed flow at the blunt trailing edge.

1.3.1 Separation at the high-lift condition

As a requirement of lower weight and higher thrust-wight ratio, engine blades tend to have higher lift curve which adds the risk of flow separation and stall. In the case of separation, the flow undergoes an unsteady behaviour characterised by a flow detachment between the suction side and pressure side of the airfoil. This unsteady flow separation is a source of noise called screech, as well as the mechanical and thermal fatigue of the blades. In addition, by affecting the wake, instability in the front blade row may interfere with the operating state of the trailing blade rows.

Gioria et al. recorded the unsteady eigenmode of airfoil flow under the condition of low Reynolds number laminar incompressible in [18]. The flow topology in laminar conditions was also studied by Rodríguez and Theofilis [19] over a separated airfoil. The results of the study in the turbulent flow regime was recorded by Wales et al. [20] [21]. Wherein they conducted stability analysis on a stalled NACA0012 airfoil at a high angle of attack and they applied continuous simulations with a changing angle of attack on base flow. An unstable model was documented just after the Cl_{max} condition. Besides, they found the rightmost eigenvalues of the system that determined the global stability.

1.3.2 Base bleed at the transonic blunt trailing edge

As a matter of fact that the trailing edge of turbine blades is designed to be blunt, the flow at the end of the turbine blade undergoes a low momentum and low-pressure area, which is known for the base region, resulting in flow separation and unsteadiness. Besides, turbomachinery airfoils typically operate in transonic or supersonic flow conditions, which causes aero-structural coupling leading to structural fatigue and reduced efficiency. Furthermore, because of the relatively thin edge of trialling edge and high pressure&temperature condition blades endure, cooler flow bleeding is withdrawn from the high-pressure compressor and purged from the surface of turbine blades. This cooling bleed can also be adopted in controlling the flow properties of the base zone (shown in studies [22] [23]).

In the year of 1985, Kost, F. H., and Holmes, A. T., [24] documented the base bleed regime at the rear part of transonic rotor blades. In 1995, Bohn, D. E. et. al [25] investigated a guide vane case using experimental and numerical methods. Breakthroughs didn't appear until 2013, when Saracoglu, B. H. et. al [26] studied the flow topology as a function of the intensity of base bleeding flow, in supersonic regime. He found an asymmetric flow configuration characterised by pressure bifurcations in symmetric nodes.

1.3.3 Aims of the study

This study aims to analyse the high-lift separation and non-symmetric flow topology of base bleeding using both RANS equations solver and linear stability analysis theory. With TAU numerical tools, flow topologies are obtained by solving RANS equations, a simplified approach of compressible Navier-Stokes equations. Then the BiGlobal stability analysis is conducted to identify the mode leading to unsteady configuration.

1.4 Organization of the thesis

The methodology adopted by the study is introduced in Chapter 2, containing the theory and numerical tools of base flow computation and linear analysis. A validation case of cylinder flow is also described at the end of this chapter. The results and analysis of high-lift case and transonic base bleed case are shown in Chapter 3 and Chapter 4 respectively. Future work and conclusion are put forward in Chapter 5 finally.

Chapter 2

Methodology

2.1 Base flow computation

2.1.1 Governing equations

The governing equations of the fluid motion can be described as the conservation of mass, momentum, and energy. Most generally, the fluid motion is governed by the time-dependent three-dimensional compressible Navier-Stokes system of equations. For a viscous Newtonian, isotropic fluid without external forces or heat, mass diffusion and finite-rate chemical reactions, the strong conservation form of the Navier-Stokes system of equations can be written as:

$$\begin{aligned} \tfrac{\partial \rho}{\partial t} + \nabla \cdot (\rho g) &= 0 \\ \tfrac{\partial (\rho u)}{t} + \nabla \cdot (\rho u u) &= -\nabla p + \nabla \cdot \rho \\ \tfrac{\rho e_t}{\partial t} + \nabla \cdot (\rho e_t u) &= k \nabla \cdot \nabla T - \nabla p \cdot u + (\nabla \cdot \rho) \cdot u \end{aligned} \tag{2.1}$$

The vector form of this set of equations is:

$$\frac{\partial Q}{\partial t} + \frac{\partial E_i}{\partial x} + \frac{\partial F_i}{\partial y} + \frac{\partial G_i}{\partial z} = \frac{\partial E_v}{\partial x} + \frac{\partial F_v}{\partial y} + \frac{\partial G_v}{\partial z} \tag{2.2}$$

where Q represents the vector of the flow variables as:

$$Q = \begin{bmatrix} \rho \\ \rho u \\ \rho v \\ \rho w \\ \rho e_t \end{bmatrix} \tag{2.3}$$

The vectors $E_i = E_i(Q)$, $F_i = F_i(Q)$ and $G_i = G_i(Q)$ containing the inviscid fluxes in the x, y and z directions are given as flows:

$$E_i = \begin{bmatrix} \rho u \\ \rho u^2 + p \\ \rho u v \\ \rho u w \\ (\rho e_t + p) u \end{bmatrix}, F_i = \begin{bmatrix} \rho v \\ \rho v u \\ \rho v^2 + p \\ \rho v w \\ (\rho e_t + p) v \end{bmatrix}, G_i = \begin{bmatrix} \rho w \\ \rho w u \\ \rho w v \\ \rho w^2 + p \\ (\rho e_t + p) w \end{bmatrix} \tag{2.4}$$

where u is the velocity vector including the u, v and w velocity components in the Cartesian coordinate and p, ρ and e_t represent the pressure, density and total energy per unit mass respectively.

In addition, $E_v = E_v(Q)$, $F_v = F_v(Q)$ and $G_v = G_v(Q)$ are vectors containing the viscous fluxes in the x, y and z directions given as follows:

$$
\begin{aligned}
E_v &= \begin{bmatrix} 0 \\ \tau_{xx} \\ \tau_{xy} \\ \tau_{xz} \\ u\tau_{xx} + v\tau_{xy} + w\tau_{xz} - q_x \end{bmatrix} \\
F_v &= \begin{bmatrix} 0 \\ \tau_{yx} \\ \tau_{yy} \\ \tau_{yz} \\ u\tau_{yx} + v\tau_{yy} + w\tau_{yz} - q_y \end{bmatrix} \\
G_v &= \begin{bmatrix} 0 \\ \tau_{zx} \\ \tau_{zy} \\ \tau_{zz} \\ u\tau_{zx} + v\tau_{zy} + w\tau_{zz} - q_z \end{bmatrix}
\end{aligned}
\tag{2.5}
$$

where the heat fluxes q_x, q_y and q_z are defined by the Fourier's law of heat conduction as follows

$$
\begin{aligned}
q_x &= -k\frac{\partial T}{\partial x} \\
q_y &= -k\frac{\partial T}{\partial y} \\
q_z &= -k\frac{\partial T}{\partial z}
\end{aligned}
\tag{2.6}
$$

and the viscous stresses $\tau_x x$, $\tau_y y$, $\tau_z z$, $\tau_x y$, $\tau_y x$, $\tau_x z$, $\tau_z x$, $\tau_y z$ and $\tau_z y$, are given by the following relationships

$$
\begin{aligned}
\tau_{xx} &= \tfrac{2}{3}\mu(2\tfrac{\partial u}{\partial x} - \tfrac{\partial v}{\partial y} - \tfrac{\partial w}{\partial z}) \\
\tau_{yy} &= \tfrac{2}{3}\mu(2\tfrac{\partial v}{\partial y} - \tfrac{\partial u}{\partial x} - \tfrac{\partial w}{\partial z}) \\
\tau_{zz} &= \tfrac{2}{3}\mu(2\tfrac{\partial w}{\partial z} - \tfrac{\partial u}{\partial x} - \tfrac{\partial v}{\partial y}) \\
\tau_{xy} &= \mu(\tfrac{\partial u}{\partial y} + \tfrac{\partial v}{\partial x}) \\
\tau_{xz} &= \mu(\tfrac{\partial u}{\partial z} + \tfrac{\partial w}{\partial x}) \\
\tau_{yz} &= \mu(\tfrac{\partial v}{\partial z} + \tfrac{\partial w}{\partial y}) \\
\tau_{yx} &= \tau_{xy} \\
\tau_{zx} &= \tau_{xz} \\
\tau_{zy} &= \tau_{yz}
\end{aligned}
\tag{2.7}
$$

where μ is the laminar viscosity

Examining Eq. 2.1-2.4, it is clear to see that there are five equations in terms of seven flow field variables u, v, w, ρ, p, T, and e_t. Two additional equations are required to close the equation system. These two additional equations can be obtained by proposing the equations of state. With a reasonable assumption that the intermolecular forces inside the working gas are negligible, known as the perfect gas assumption, the equation of state is given as:

$$p = \rho R_g T \tag{2.8}$$

where R_g equals to $287m2/s^2K$ for air, known as the specific gas constant

With the additional assumption that the working gas behaves with constant specific heats, known as a calorically perfect gas [27], then the following relations are given as

$$e_i = c_v T, h = c_p T, \gamma = \frac{c_p}{c_v}, c_v = \frac{R_g}{\gamma - 1}, c_p = \frac{\gamma R_g}{\gamma - 1} \tag{2.9}$$

where γ equals 1.4 for air, known as the ratio of specific heats. C_v, c_p, h represent the specific heat at constant volume, specific heat at constant pressure and enthalpy respectively.

Furthermore, the transport properties (μ, k) is ought to be related to thermodynamic variables as follows:

The laminar viscosity μ is determined by Sutherland's formula:

$$\mu = \frac{C_1 T^{\frac{3}{2}}}{T + C_2} \tag{2.10}$$

where the constants for air are $C_1 = 1.458 \times 10^{-6} \frac{kg}{ms\sqrt{K}}$ and $C_2 = 110.4K$.

The thermal conductivity of the fluid, k, is computed with the Prandtl number ($Pr = 0.72$ for air)as

$$K = \frac{c_p \mu}{Pr} \tag{2.11}$$

where c_p and mu are given by equations Eq. 2.9 and Eq. 2.12 respectively.

It is necessary to notice that the Navier-Stokes system of equations Eq. 3.1, Eq. 3.2, Eq. 3.3 and Eq. 3.4, is a coupled system of non-linear partial differential equations (PDE), which is very difficult to solve analytically. It is common to adopt RANS with turbulence model approach to compute the solution [28] [29].

2.1.2 RANS equations

The Reynolds average NS equation is the governing equation of the flow field mean variables, and its related simulation theory is called the turbulence model theory. The turbulence model theory assumes that the flow field variables in turbulence consist of time-averaged quantities and pulsating quantities. From this point of view, the NS equation can be derived as the Reynolds average NS equation (referred to as the RANS equation).

$$\begin{aligned}
\frac{\partial \rho}{\partial t} + div(\rho u) &= 0 \\
\frac{\partial(\rho u)}{\partial t} + div(\rho u u) &= div(\mu grad u) - \frac{\partial p}{\partial x} + \left[-\frac{\partial(\rho \overline{u'^2})}{\partial x} - \frac{\partial(\rho \overline{u'v'})}{\partial y} - \frac{\partial(\rho \overline{u'w'})}{\partial z} \right] + S_u \\
\frac{\partial(\rho v)}{\partial t} + div(\rho v u) &= div(\mu grad v) - \frac{\partial p}{\partial y} + \left[-\frac{\partial(\rho \overline{u'v'})}{\partial x} - \frac{\partial(\rho \overline{v'^2})}{\partial y} - \frac{\partial(\rho \overline{v'w'})}{\partial z} \right] + S_v \\
\frac{\partial(\rho w)}{\partial t} + div(\rho w u) &= div(\mu grad w) - \frac{\partial p}{\partial x} + \left[-\frac{\partial(\rho \overline{u'w'})}{\partial x} - \frac{\partial(\rho \overline{v'w'})}{\partial y} - \frac{\partial(\rho \overline{w'^2})}{\partial z} \right] + S_w
\end{aligned} \tag{2.12}$$

If the indicator symbol is used in the tensor, it can be also described as:

$$\begin{aligned}
\frac{\partial \rho}{\partial t} \frac{\partial}{\partial x_i}(\rho u_i) &= 0 \\
\frac{\partial}{\partial t}(\rho u_i) + \frac{\partial}{\partial x_j}(\rho u_i u_j) &= -\frac{\partial p}{\partial x_i} + \frac{\partial}{\partial x_j}(\mu \frac{\partial u_i}{\partial x_j} - \rho \overline{u_i' u_j'} + S_i
\end{aligned} \tag{2.13}$$

The $-\overline{u_i' u_j'}$ in the above formula is called Reynolds stress, given by:

$$\tau_{ij} = -\overline{u_i' u_j'} \tag{2.14}$$

This nonlinear Reynolds stress term requires additional modelling to close the RANS equation for solving and has led to the creation of many different turbulence models.

After introducing the Boussinesq hypothesis, the turbulent Reynolds stress should be proportional to the turbulence, and the turbulence calculation is attributed to the calculation of the proportional coefficient between the Reynolds stress and the strain, that is the turbulent viscosity coefficient. It is precise because the governing equations are statistically averaged that they do not need to calculate the turbulent pulsations of each scale, and only need to calculate the average motion, thereby reducing the spatial and temporal resolution and reducing the computational workload. According to the number of variables used in the calculation and the number of equations, the turbulence model included in the turbulence model theory is divided into two categories: the two-equation model, the one-equation model, and the zero-equation model (algebraic model).

2.1.3 RANS solver

The solver TAU (version 2013.2.0), developed by DLR, is a finite-volume code in order to solve the system of equations (2.1-2.3). First, the set of equations is rewritten in conservative form as follows:

$$\frac{\partial}{\partial t} \int_\Omega q d\Omega = -\int_{\partial\Omega} \bar{F} \times n dS \tag{2.15}$$

Similar to Eq.1.3, in this case, the vector of variables q is defined as:

$$q = \begin{bmatrix} \rho \\ \rho u \\ \rho v \\ \rho w \\ \rho e_t \\ \rho \nu \end{bmatrix} \tag{2.16}$$

and Ω is the entire basin control volume with a boundary of $\partial\Omega$ and an external normal of n. Due to the spatial discretization of the finite volume [30] method, the

change in flow conditions in the control volume Ω is given by the normal component of the flux through the control volume boundary $\partial\Omega$.

The flux density tensor $\bar{F}$ can be decomposed in the Cartesian coordinate as:

$$\bar{F} = E\overrightarrow{e_x} + F\overrightarrow{e_y} + G\overrightarrow{e_z} \tag{2.17}$$

It can also be written with an introduction of inviscid and viscous fluxes defined in Eq. 1.4 and Eq. 1.5:

$$\begin{aligned}
E = E_i + E_v &= \begin{bmatrix} \rho u \\ \rho u^2 + p \\ \rho uv \\ \rho uw \\ (\rho e_t + p)u \end{bmatrix} - \begin{bmatrix} 0 \\ \tau_{xx} \\ \tau_{xy} \\ \tau_{xz} \\ u\tau_{xx} + v\tau_{xy} + w\tau_{xz} - q_x \end{bmatrix} \\
F = F_i + F_v &= \begin{bmatrix} \rho v \\ \rho vu \\ \rho v^2 + p \\ \rho vw \\ (\rho e_t + p)v \end{bmatrix} - \begin{bmatrix} 0 \\ \tau_{yx} \\ \tau_{yy} \\ \tau_{yz} \\ u\tau_{yx} + v\tau_{yy} + w\tau_{yz} - q_y \end{bmatrix} \\
G = G_i + G_v &= \begin{bmatrix} \rho w \\ \rho wu \\ \rho wv \\ \rho w^2 + p \\ (\rho e_t + p)w \end{bmatrix} - \begin{bmatrix} 0 \\ \tau_{zx} \\ \tau_{zy} \\ \tau_{zz} \\ u\tau_{zx} + v\tau_{zy} + w\tau_{zz} - q_z \end{bmatrix}
\end{aligned} \tag{2.18}$$

From Eq. 2.15 and for a temporal and spacial fixed control volume, $\partial q/\partial t$ can be defined as:

$$\frac{\partial q}{\partial t} = -\frac{1}{|\Omega|}\int_{\partial\Omega} \bar{F}\cdot n dS = -\frac{1}{|\Omega|}U^F \tag{2.19}$$

Where U^Frepresents the flux through the boundary of control volume Ω. The dual mesh is used to discretize the flow domain Ω into a finite number of subdomains Ω_i, where each subfield contains N faces. In order to compute the time variation of the flow in the control volume, convective fluxes on the control volume boundary must be determined. To solve the equation, the time variation of the flow is written in subdomain i in the general form, as follows:

$$\frac{\partial q_i}{\partial t} = -\frac{1}{|\Omega_i|}\sum_{j=1}^{N} U_j^F \tag{2.20}$$

In the steady state case, this problem is solved by introducing a corresponding time-dependent problem with a pseudo-time τ and seeking its steady-state solution. Time integration is performed using the low storage K-step Runge-Kutta scheme. Eq. 1.20 becomes:

$$\Omega_i\frac{\partial \bar{q}_i}{\partial \tau} = -R_i = \sum_{j=1}^{N} U_j^F \tag{2.21}$$

Where R_i represents the residual and q_i a particular steady solution of the problem for the subdomain i. The dimensions of vectors R_i and q_i depends on the dimensions of the case studied, such as 2D laminar case, 2D turbulent case or 3D turbulent case.

The boundary conditions on the body surface are defined as:

$$u = v = w = 0, \nu = 0, \frac{\partial T}{\partial n} = \frac{\partial \rho}{\partial n} = 0 \tag{2.22}$$

Where n represents the normal direction of the surface of the body. The far-field boundary condition is enacted on external boundaries. The AUSM Riemann solver [30] is used to calculate the flux through the far-field boundary surface, and the Whitfield theory [31] is adapted to identify the flow conditions outside the boundary. Symmetric boundary conditions are used for lateral boundaries in the 3D case.

2.2 Linear stability analysis

2.2.1 Linear stability theory

The linear stability analysis is based on a Navier-Stokes solution, namely the base flow solution. In this work particularly, the solution is the result of a RANS equation with a turbulent model. The theory analysis the eve lotion of a tiny perturbation added into the base flow. According to the Lyapunov definition, base flow is stable if an infinitesimal change only changes an infinitesimal amount of the base flow topology at a later time.

$$||U(\bar{x}, 0) - U^*(\bar{x}, 0)|| < \delta \rightarrow ||U(\bar{x}, t) - U^*(\bar{x}, t)|| < \epsilon \tag{2.23}$$

In addition, it is defined as asymptotically stable if it converges to the original solution.

$$||U(\bar{x}, t) - U^*(\bar{x}, t)|| \rightarrow 0, \quad as \quad t \rightarrow \infty \tag{2.24}$$

With the definition of q in Eq. 2.16, it is possible to rewrite the Eq. 2.1 as

$$\frac{\partial}{\partial t} M[q] + Q[q] + N[q, q] = 0 \tag{2.25}$$

Where M and Q are linear operators and N contains all nonlinear terms. Linear analysis decomposes base flow variables $q(x, t)$ into steady base flow $\bar{q}$ and unsteady small amplitude perturbations q_0 as

$$\begin{gathered} q(x, t) = \bar{q}(x) + \epsilon q'(x, t), \qquad \epsilon << 1 \\ as \frac{\partial \bar{q}}{\partial t} = 0 \end{gathered} \tag{2.26}$$

With Eq. 2.25 minus Eq. 2.26, the linearized equations of q' gives as

$$\frac{\partial}{\partial t} M[q'] + N_{\bar{q}}[q'] = 0 \tag{2.27}$$

Where M contains terms related to the time derivative, while $N_{\bar{q}}$ contains linear terms from the original equation and terms resulting from nonlinear interactions between $\bar{q}$ and q'. These operators are associated with spatial discretization of linear N-S equations and include the basic state $\bar{q}$ and its spatial derivative.

2.2.2 Model stability analysis

Model linear stability analysis introduces the mode perturbations with seperated space&time terms defined as:

$$q'(x,t) = \hat{q}(x)exp(-i\omega t) \tag{2.28}$$

Substituted in Eq. 2.26, the linearized equations of $\hat{q}$ is given as:

$$A\hat{q} = \omega B\hat{q} \tag{2.29}$$

Where A and B represent the discretized form of M and $N_{\bar{q}}$. In compressible regime, B is not singular and the equation can be rewritten as

$$C\hat{q} = \omega\hat{q} \tag{2.30}$$

where C is defined as: $C = B^{-1}A$

The objective of the model linear stability theory is to compute the eigenvalue ω and the eigenvector q as Eq. 2.30 with q describes the mode shape and characterizes the evolution of the tiny perturbations. C depends on properties of base flow computation such as Reynolds number, mesh, etc.

The linearized form of the N-S equations is valid when the perturbation amplitude is small enough to make the non-linear terms negligible.

2.2.3 Stability analysis solver

The aligned solver TAUev (version 2013.2.0), developed by DLR, is adopted to solve the stability analysis problem.

Eq. 2.20 and Eq. 2.21 can be rewritten in compact form as

$$B\frac{\partial q}{\partial t} = R(q) \tag{2.31}$$

where B is the diagonal matrix defined in Eq. 2.29 and R is the discrete N-S operator. Substituting the Eq. 2.25 with q, the equation can be rewritten as

$$\epsilon B\frac{\partial q'}{\partial t} = R(\bar{q} + \epsilon q') \approx R(\bar{q}) + \epsilon \left[\frac{\partial R}{\partial q}\right]_{\bar{q}} q' \tag{2.32}$$

Noticing that $\bar{q}$ is a particular solution of RANS equation, which means $R(\bar{q}) = 0$, the equation is therefore transformed into a real-valued eigenvalue problem for determining the real number of ω:

$$\left[\frac{\partial R}{\partial q}\right]_{Q} \hat{q} = \omega B\hat{q} \tag{2.33}$$

which is equivalent to Eq. 2.29 as $A = \left[\frac{\partial R}{\partial q}\right]_{\bar{q}}$ known as the Jacobian of the system. It is computed once a steady solution of RANS equation is obtained, corresponding to the linearization of the discrete N-S operator R over the base flow $\bar{q}$.

Once the matrix A is computed, TAUev uses the Arnoldi algorithm [32] [33] to solve the eigenvalue problem, as shown briefly in Table 2.1.

Arnoldi algorithm
1. Compute $\hat{A} = A - B\sigma$ and overwrite $\hat{A}$ by its LU decomposition
2. Choose an initial random vector v_1 and normalise it
3. Compute the entries h_ij of the Hessenberg matrix
For $j = 1, 2...m$ do
Set $\omega_j = (B, v_j)$
Solve $\hat{A}x = \omega_j$
For $i = 1, 2...j$ do
Form $h_{ij} = (v_i, x)$,
Form $x = x - hijv_i$
Normalize $h_{j+1,j} = \|X\|$
Form $v_{j+1} = \frac{x}{h_{j+1,j}}$
4. Compute the eigenvalues and the eigenvectors of H_m using the QZ algorithm
5. Compute the Ritz vectors $\hat{q}_i = (V_m, y_i^m)$

TABLE 2.1: Arnoldi algorithm process

2.3 Validation case: vortex shedding from a cylinder

In this section, a case of vortex shedding onset on a circular cylinder is studied with the methodology described in the previous sections. The case is perfectly discussed in [34] [35], which has been wildly used as reference solutions. In a certain range of Reynolds number, the eddy produced by the boundary layer separation fall off from either side of the cylinder periodicity, which is known as Von Karman vortex street. The purpose of this work is to prove the accuracy of the base flow calculation and the effectiveness of the stability analysis.

2.3.1 Simulation settings

A quasi-3D structured typical mesh (shown in Figure 2.1) is adopted in this case, with a diameter of the circular cylinder $d = 1$, and the centre of the circle situated in point (0,0,0). The computation domain is defined as a rectangle with points (-20,0,-20), and (50,0,20). There are 36036 nodes constructing 36000 quadrilateral elements, refined at the rear of the cylinder, considering the cylinder wake.

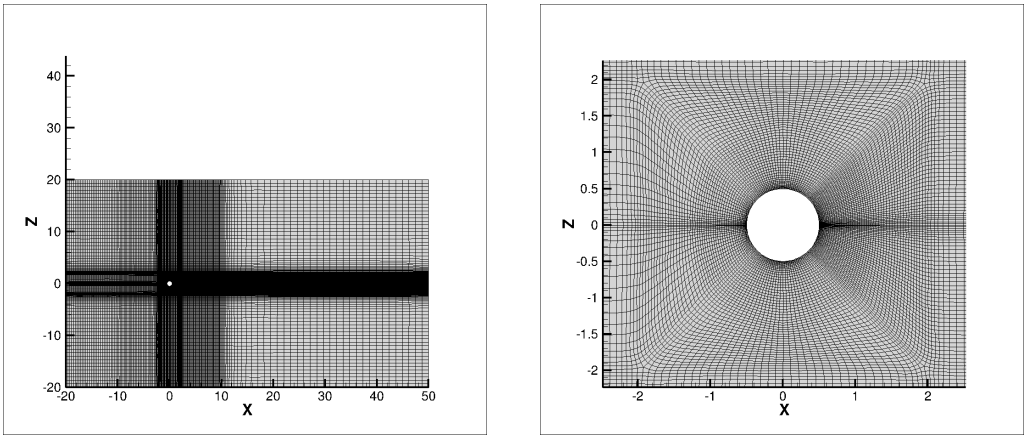

(A) overall view (B) detailed view

FIGURE 2.1: general and detailed view of the mesh used for validation case.

As is well known in work of literature, the critical Reynolds number of the onset of Von Karman vortex street $Re_{cr} \approx 47$. The base flow is computed under the Reynolds number $Re = 60$, when the unsteadiness is fully developed. Considering of the incompressible flow regime, a Mach number $Ma = 0.2$ is chosen. Other parameters are chosen considering the perfect gas and standard atmosphere assumptions (shown in Table 2.2). For the boundary conditions, far-field and no-slip boundary types are chosen for the external boundary of the computing domain and internal boundary of the domain (the boundary of the cylinder) respectively. Detailed flow settings are shown in appendix A.

Perfect gas thermodynamic	
Gas constant R	287
Gas constant gamma	1.4
Transport coefficients	
Prandtl number	0.72
Sutherland constant	110.4

References	
Reynolds length	0.160
Reference Mach number	0.7
Reference pressure	101325
Reference temperature	391.62

TABLE 2.2: coeffiecients used in the cylinder case

2.3.2 Simulation process

The first step is the base flow calculation with TAU solver, that unsteady flow simulation is selected due to the flow instability. Meanwhile, apart from the standard monitoring process of parameters of the whole body, a profiling process is conducted to monitor changes in flow variables at specific several (10 in this case) points.

To verify the base flow results, the next step is analysing the monitoring file and extract the amplitude of the oscillation with the FFT (Fast Fourier Transfer) process. Then the Strouhal Number, a standard parameter for turbulence, is calculated with the cylinder diameter D and the free stream velocity U as $St = \frac{D \times f}{U}$. Finally, the result is compared with empirical results.

As preparation for stability analysis, a mean flow solution is obtained when the non-steady state is fully developed characterised by the periodic changes of flow variables. Because the stability analysis can only be effective on the basis of a stable base flow result. In fact, it is also adaptable to perform a steady simulation, forcing the result to converge to a steady state with a specific residual and consequently suitable for stability analysis, which is performed in the airfoil case in chapter 3.

For instability analysis, the TAUev tools are applied to extract the Jacobian matrix on the basis of the mean flow result and plot the eigenvalue of the flow. With a view of the eigenvalue map, suspicious points are selected and the corresponding eigenvectors, eigenmodes of the flow, are decomposed and visualised.

The whole process is concluded as follows:

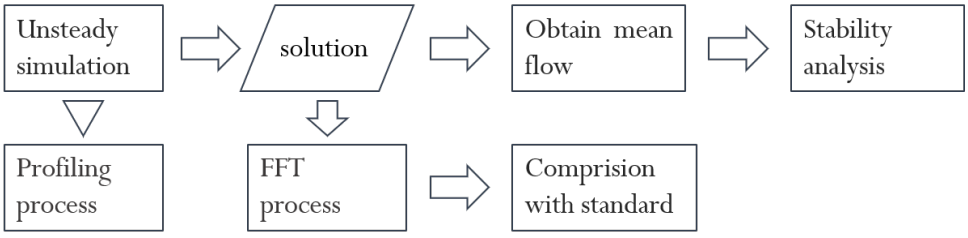

FIGURE 2.2: simulation process

2.3.3 Base flow calculation results

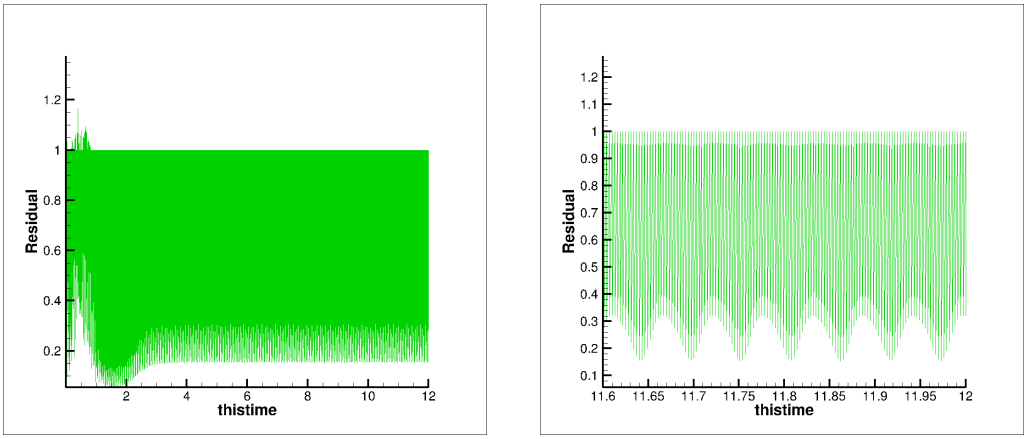

(A) overall view (B) detailed view

FIGURE 2.3: residual monitor

Figure 2.3 and Figure 2.4 illustrate the residual and lift and drag coefficient values as functions of the time step. As shown in Figure 2.3, after the fluctuation period before 4s, periodic oscillation occur throughout the iteration process. Accordingly, after this point in time, the values of the lift and drag coefficients periodically oscillate as shown in Figure 2.4..

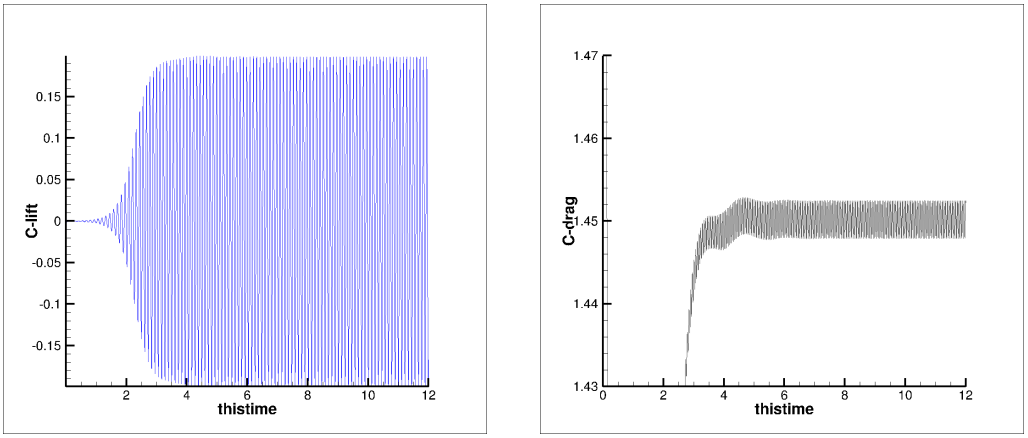

(A) C_{lift} monitor (B) C_{drag} monitor

FIGURE 2.4: C_{lift} & C_{drag} monitor

From a view of the C_life plot, the entire iterative process can be divided into three phases. They are transient, linear and saturated(periodic), the amplitude of the oscillation increase at a low rate, increase at a stable rate and remain level, respectively.

AS introduced before, the variations of velocity component in the x-direction with iteration over 10 key points are also obtained by the profiling process, as shown in Figure 2.5 below. It is noticeable that a similar pattern is manifested with the results before. After transient and linear increase periods, the value of x_velocity oscillates at a stable amplitude with the time step increasing. The results of profiling ensure the flow parameters in specific in details behave properly and aligned with the entire flow field properties.

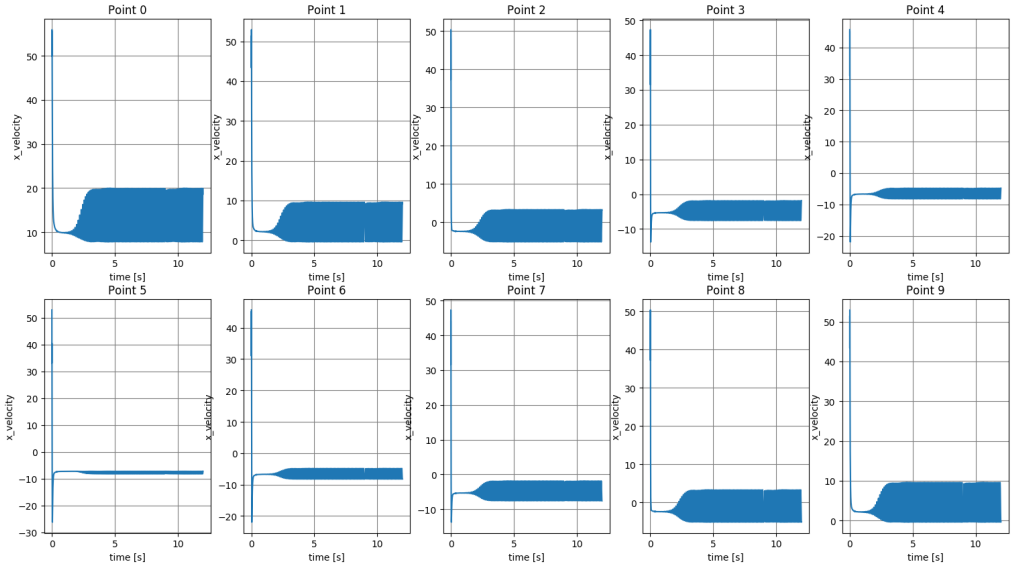

FIGURE 2.5: profiling results

As a result, the Fast Fourier Transfer(FFT) is applied from 4s to 9s to identify the oscillating frequency during the saturated period. The C_lift is chosen as the object because it experiences the simplest pattern of variation. The result of FFT is shown below and the frequency of max energy is 9.0180 and the amplitude of the oscillation is 3.8740e-01. And the Strouhal Number can be calculated according to the method mentioned before, with a result of 0.136, which is in good agreement with the empirical results for a Reynolds number of 60, as it can be consulted in many references.

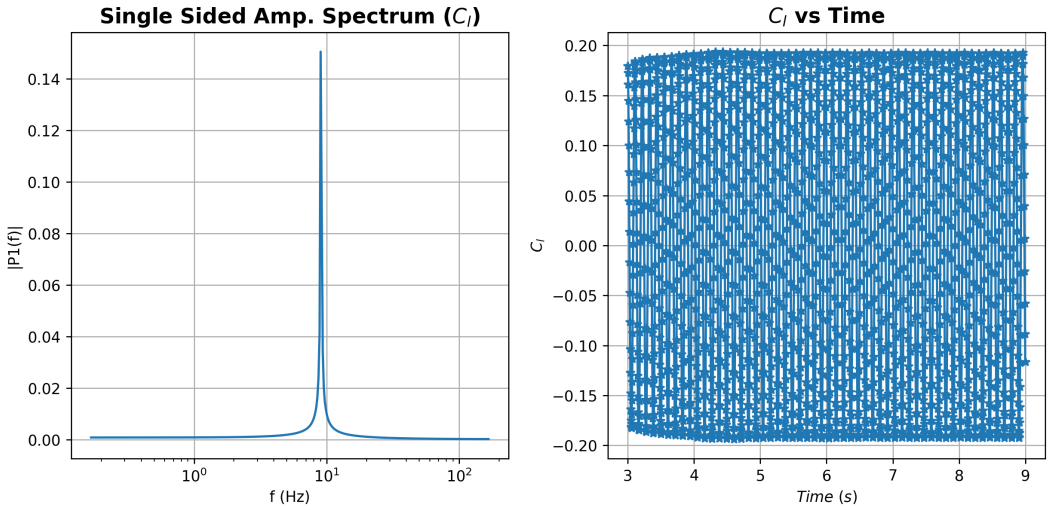

FIGURE 2.6: Results of FFT of C_{lift}

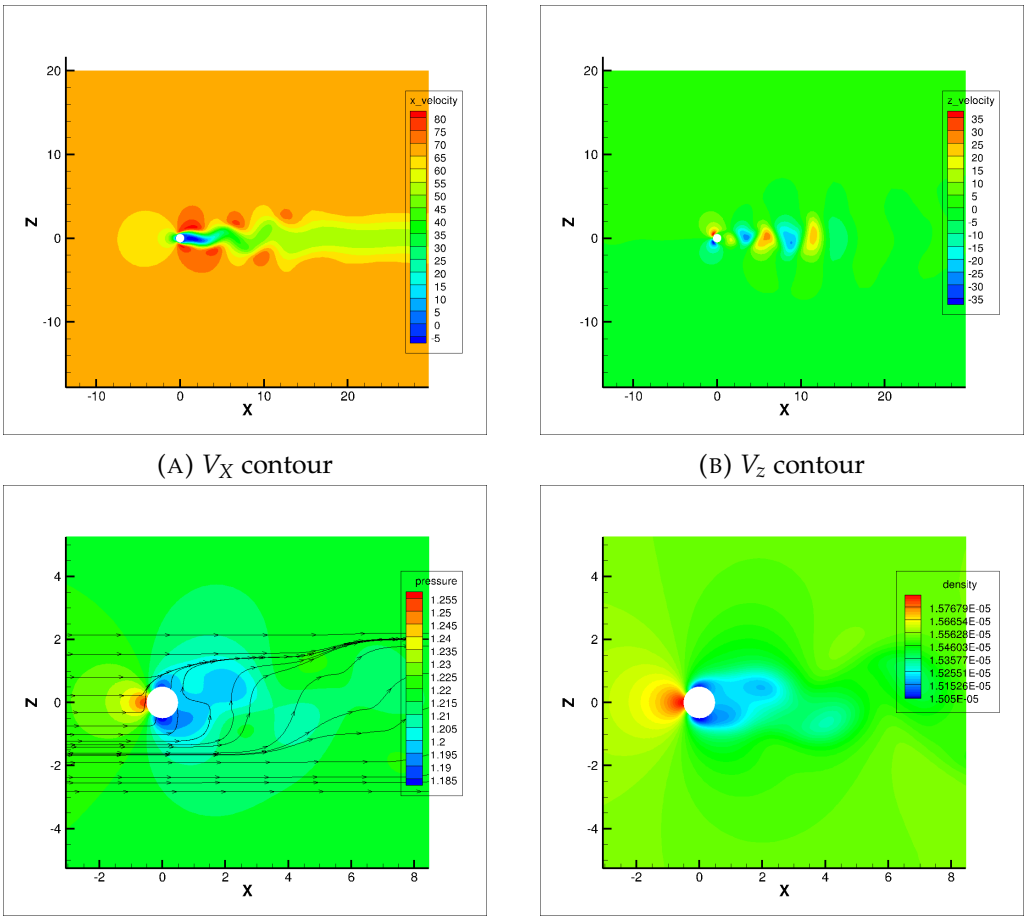

(A) V_X contour

(B) V_z contour

(C) pressure contour

(D) density contour

FIGURE 2.7: base flow contour results

The contour of the flow field of velocity components in horizontal and vertical directions are shown in Figure 2.7 above, with the contour of pressure, density and streamlines around the cylinder and at the wake area. It can be seen that the flow instability is fully developed and the Von Karmen vortex street is obvious in the x_velocity contour. The base flow results are in good agreement with the literature.

2.3.4 Stability analysis results

Using the TAU tools, the mean flow is computed from 9 to 12 seconds, during when the flow oscillates with a stable amplitude for at least 100 periods, as shown in Figure 2.3 or 2.4. The contour results of u, the horizontal component of velocity, v, the vertical component of velocity, pressure and density are shown below in Figure 2.7. The mean flow field shows a perfectly symmetry topology since the instability is symmetry over a long period.

Then, with the help of TAUev, the eigenvalue map below is extracted. In these plots, the vertical axis and the horizontal axis represent the real and imaginary parts of the eigenvalues, respectively. In particular, the value of the real part is also known for the growth rate or amplification rate. If the value is positive, the instability grows exponentially and is predicted to dominate the whole flow topology. The related eigenvector represents the unstable model accountable for the unsteadiness. Since the eigenvalue map is shown as a symmetric figure as illustrated in figure 2.8, in

spite of 2 critical points existing, only the 90^{th} point on the right side is selected and its model is obtained below.

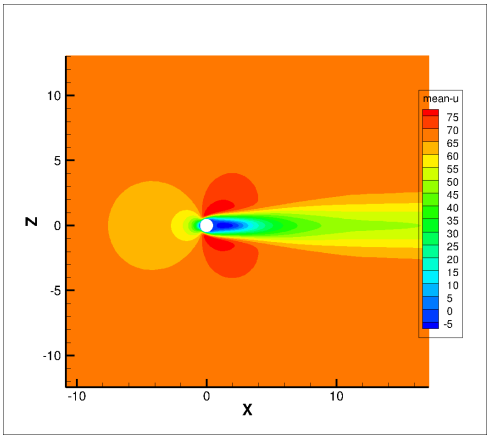

(A) mean v_x contour

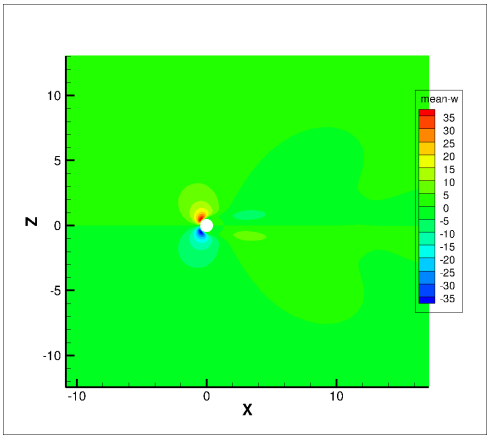

(B) mean v_z contour

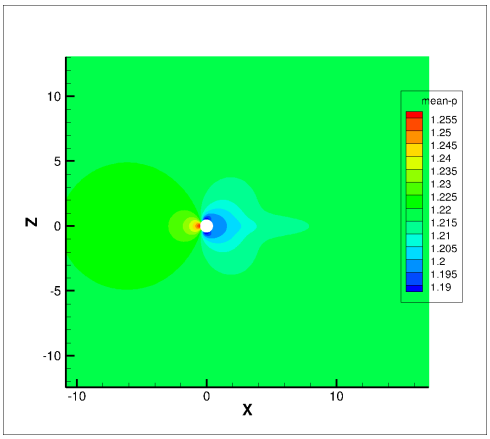

(C) mean pressure contour

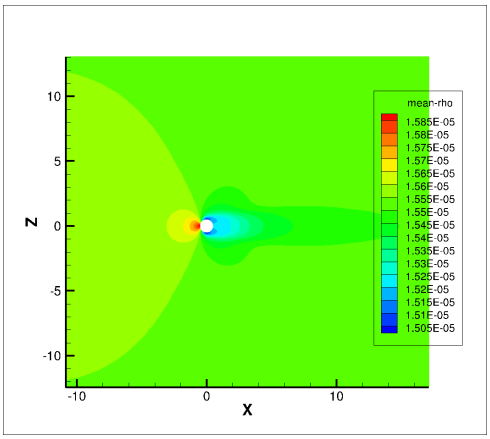

(D) mean density contour

FIGURE 2.8: mean flow results

As shown in the figures, an asymmetric model is manifested for u, x components of velocity, rho, the density and e, the energy. It is the model that affect the flow instability of cylinder flow.

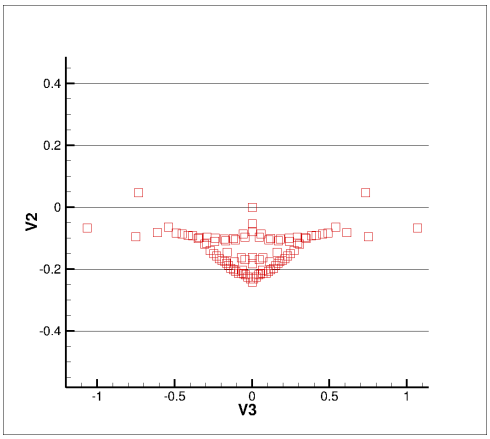

(A) total view

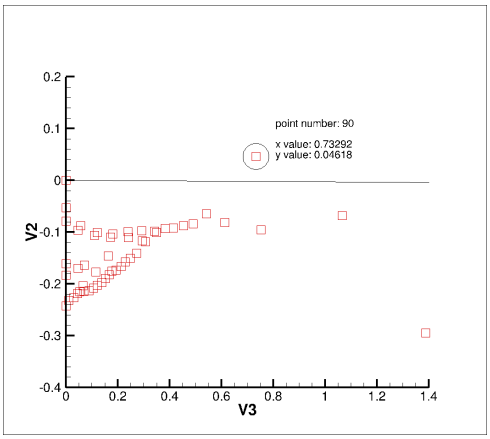

(B) detailed view

FIGURE 2.9: eigenvalue map

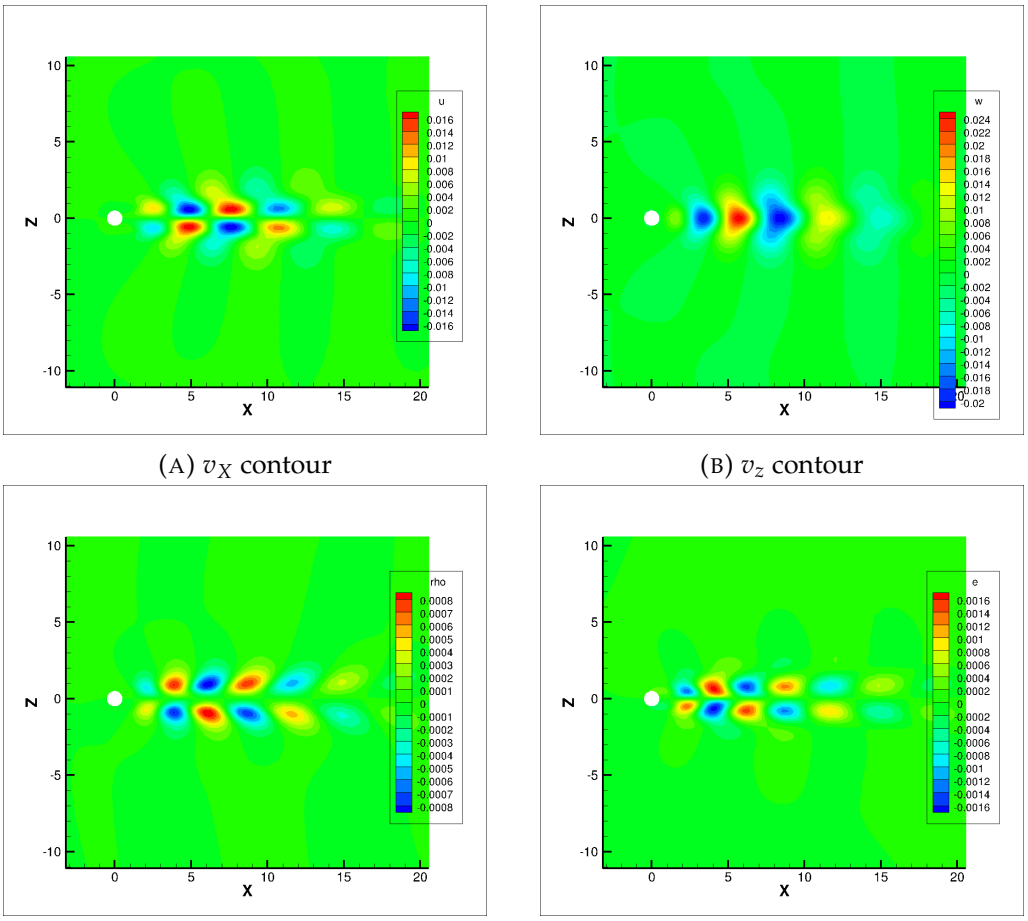

(A) v_X contour

(B) v_z contour

(C) pressure contour

(D) e contour

FIGURE 2.10: contours for unsteady model

2.3.5 Summary and conclusions

In this section, a computation of cylinder flow is proven to be accurate and the instability analysis successfully specifies the dominant model that affect the asymmetric phenomena.

Chapter 3

High angle of attack case

3.1 Simulation setting

Similar to the validation case, in this case, a quasi-three-dimensional structured grid is adopted as well, the overall and detailed view of it is shown below. The computation domain is set as circular in the x-z plane and the NACA0012 airfoil standardised with chord length is settled in the middle of it. The airfoil leading edge coordinate point is (0,0,0). And the radius of the domain $R_d = 100c$, one hundred times the chord length.

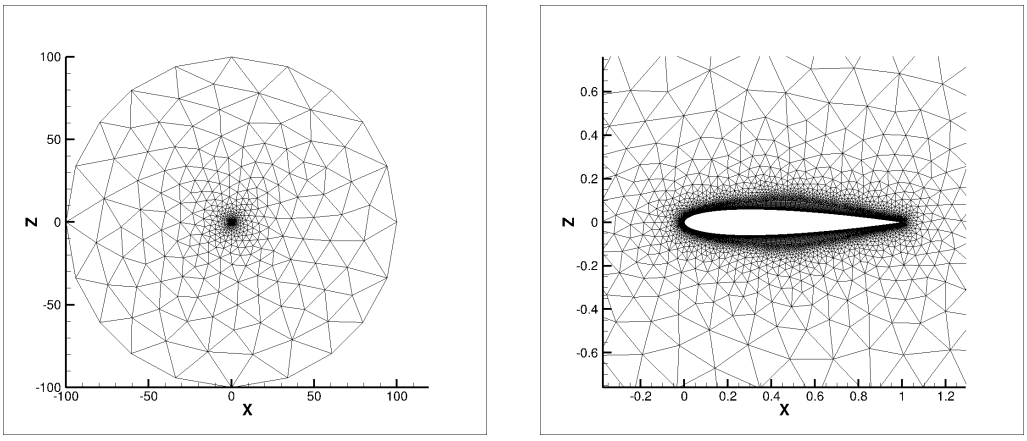

FIGURE 3.1: mesh used in airfoil case

As for the parameters chosen in this case, the flow is computed under the Reynolds number $Re = 6 \times 10^6$, with a Mach number $Ma = 0.15$ considering the subsonic condition. Other parameters are chosen according to the perfect gas and standard atmosphere theory (shown in Table 3.1). Besides, S-A turbulence model is chosen in this flow regime. The far-field boundary condition is applied at the external boundary of the domain and no-slip wall condition is enacted to the surface of the airfoil.

Perfect gas thermodynamic	
Gas constant R	287
Gas constant gamma	1.4
Transport coefficients	
Prandtl number	0.72
Sutherland constant	110.4
Sutherland reference viscosity	1.7894e-05
Sutherland reference temperature	288.15

References	
Reynolds length	0.160
Reference Mach number	0.15
Reference pressure	101325
Reference temperature	391.62
Reynolds number	6e6

TABLE 3.1: parameters used in the airfoil case

3.2 Simulation process

As illustrated in Figure 3.2, at first, the computation is set as steady, forcing the unsteadiness to converge to an acceptable residual (10^{-7} in this case), as discussed in the validation case in Chapter 2. Besides, steady simulation requires fewer memory resources and is a time saver.In the simulation, the angle of attack changes from 0 to 19 degrees and the simulation results of C_l and C_d changing with AOA is compared with experiments results from [36]. Detailed flow parameters in 18 degrees of angle of attack (as an example) are shown in Appendix A.2.

Thereafter, an unsteady simulation is performed within a narrow range of the AOA to determine an accurate critical separation point. Meanwhile, the FFT is performed to give a clue to the main model. Finally, the stability analysis of the critical angle of attack is carried out, and the main eigenmode is obtained.

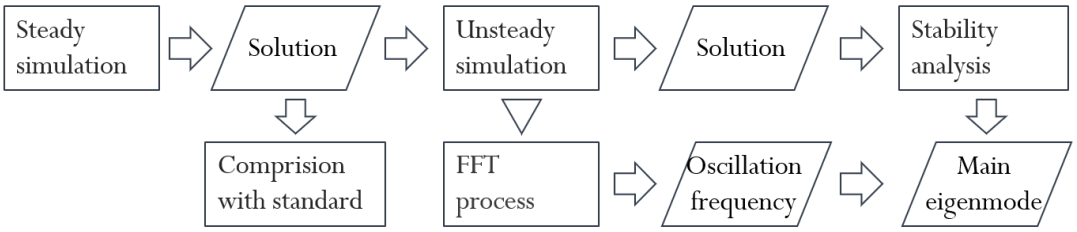

FIGURE 3.2: simulation process

3.3 Base flow results

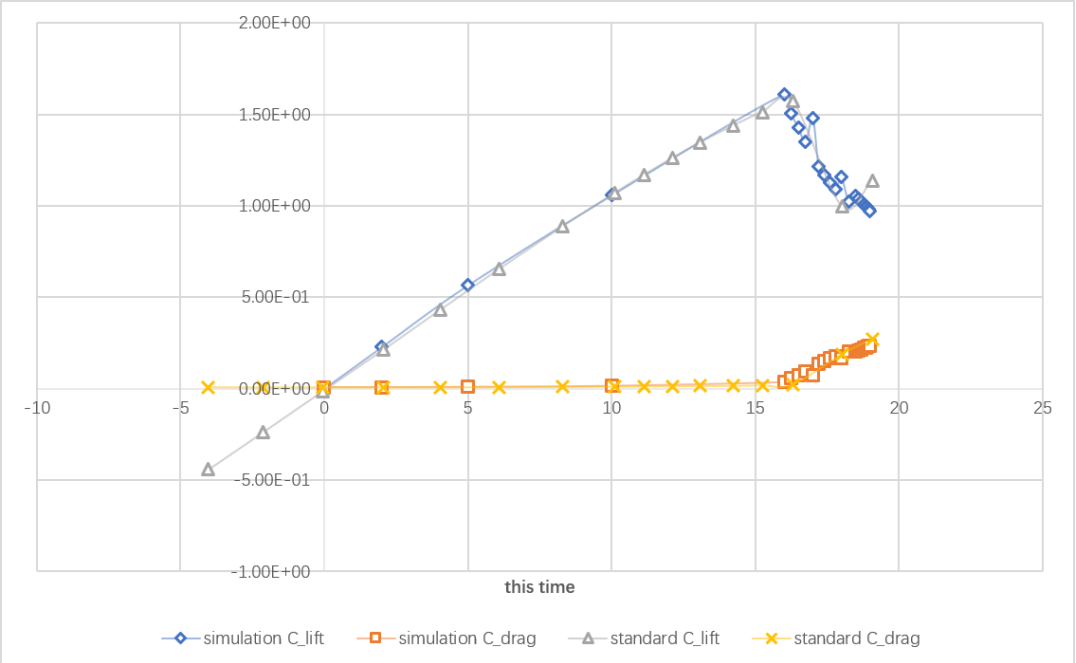

FIGURE 3.3: C_{lift} and C_{drag} monitor

Figure 3.3 shows the results of the lift and drag coefficients for the NACA0012 airfoil as a function of angle of attack. The experimental results are also plotted in the same coordinates. Obviously, in addition to the fluctuation at AOA of 17 and 18.5

degrees, where C_lift shows higher and C_drag shows lower than expected results, the simulation results are in good agreement with the experimental results.

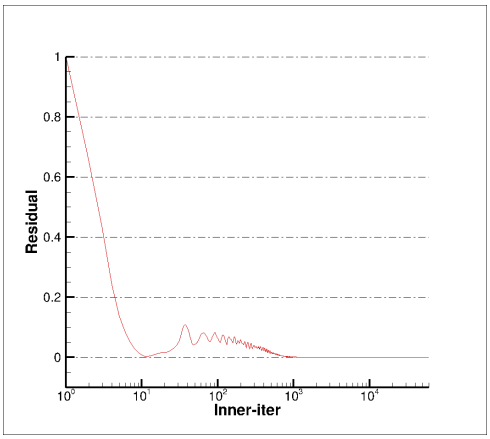

(A) residual monitor

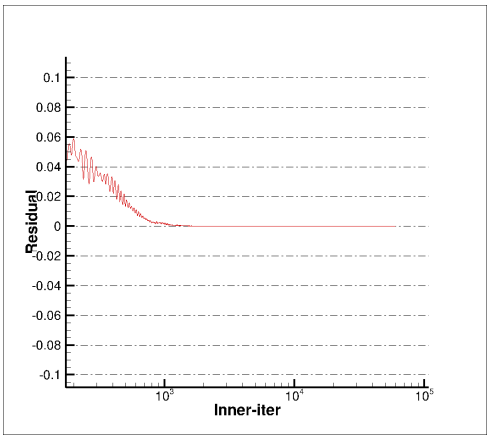

(B) residual monitor local

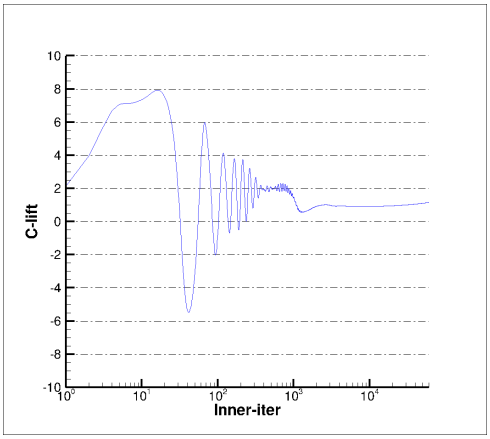

(C) C_{lift} monitor

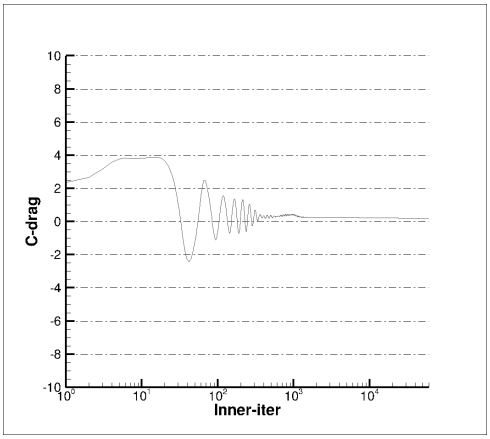

(D) C_{drag} monitor

FIGURE 3.4: parameters monitors at angle of attack of 18 degrees

Figure 3.4 shows the residual convergence plot and the lift and drag coefficient plot at an angle of attack of 18 degrees. It is worthy to point out that log coordinate is used in x-axis in order to manifest the fluctuation pattern of the data. It can be seen that the residual becomes satisfying and lift coefficient has basically converged and does not change when the iteration exceeds 10^5 times.

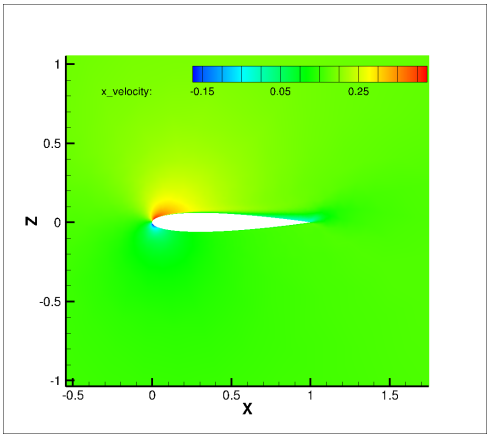

(A) angle of attack at 16 degrees

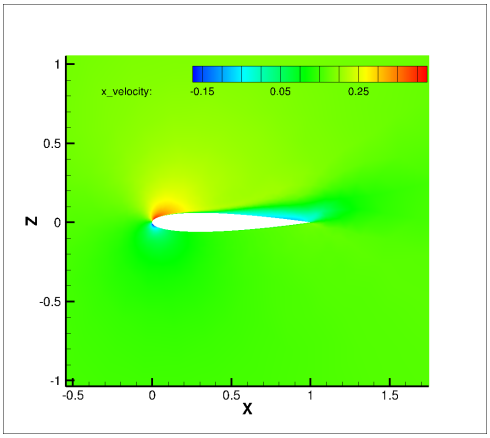

(B) angle of attack at 17 degrees

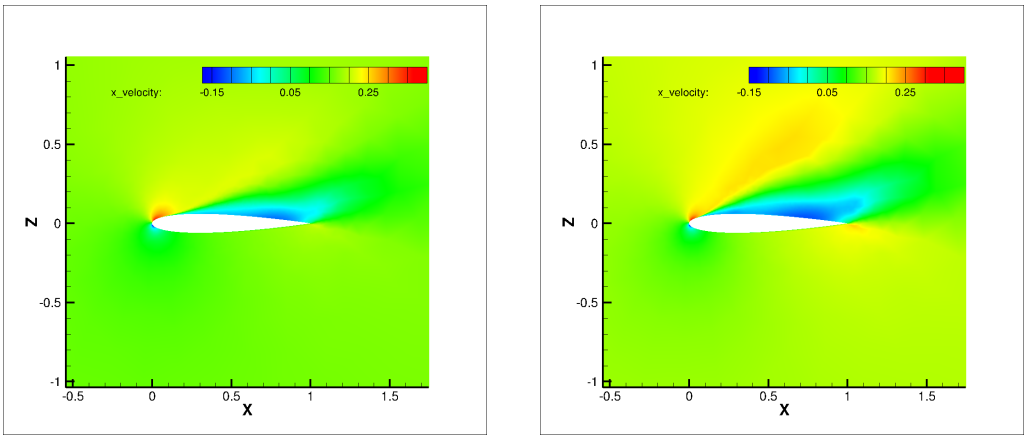

(A) angle of attack at 18 degrees (B) angle of attack at 19 degrees

FIGURE 3.6: x velocity contours

Figure 3.4 and 3.5 illustrate the contour for horizontal velocity V_x of the airfoil near the stall point, corresponding to 16 degrees, 17 degrees, 18 degrees, and 19 degrees respectively. It can be seen from the figures that when the angle of attack reach 16 degrees, the separation bubble has appeared on the trailing edge of the airfoil, with a reverse horizontal flow there. At 19 degrees, the flow has completely separated. As a result, it is speculated that the critical angle of attack for stall should be between 18 and 19 degrees.

In order to locate the critical angle of attack and instability frequency of the stall with higher accuracy, this paper performs a set of unsteady flow simulations between 18 and 19 degrees.The physical time step is set as 0.01 seconds, the simulation steps are set as 400, and the maximum iteration times at each physical step is set as 1000.

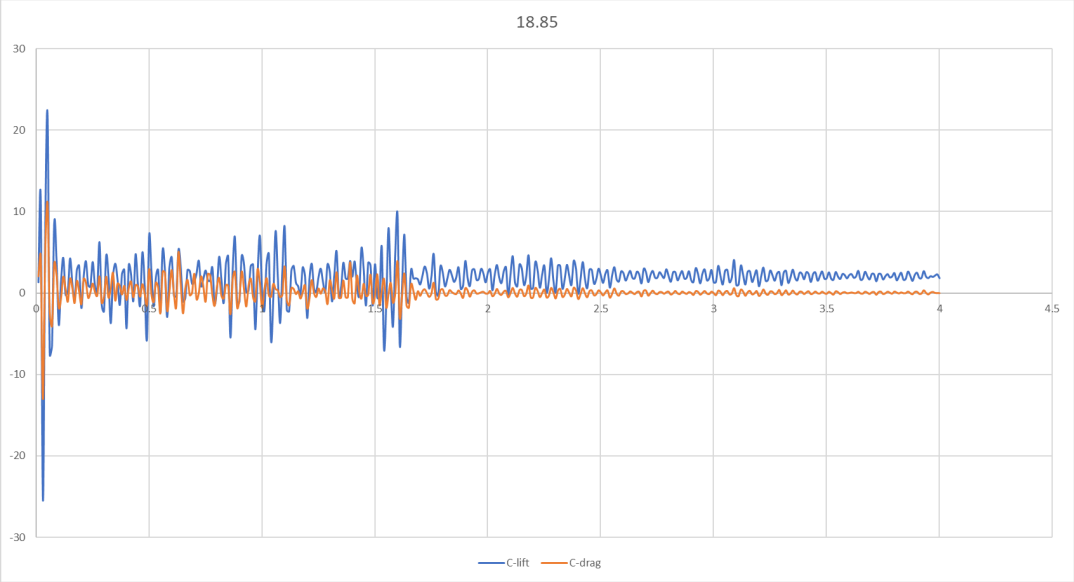

FIGURE 3.7: C_lift and C_drag at AOA 18.85

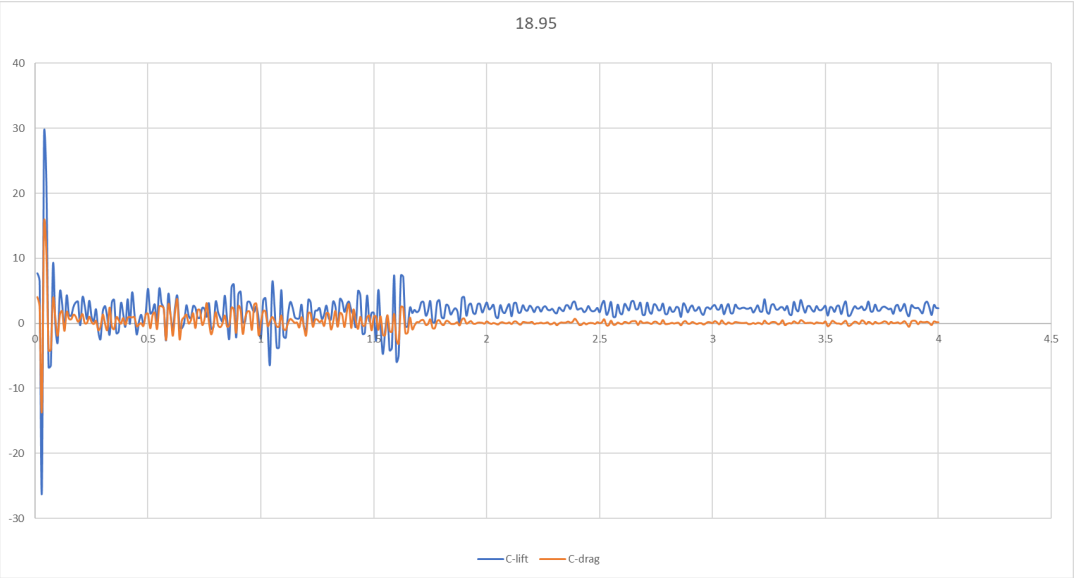

FIGURE 3.8: C_lift and C_drag at AOA 18.95

Figures 3.7 and 3.8 show the results of the lift coefficient and drag coefficient as functions of iteration time from 18.85 degrees to 18.95 degrees. At 18.85 degrees, the disturbance of the lift coefficient gradually dissipated with the data converging to a certain number as time progressed. Yet at 18.95 degrees, the lift coefficient shows a relatively stable fluctuation with a certain frequency. Therefore, the stability theory should be applied at an angle of attack of 18.9 degrees.

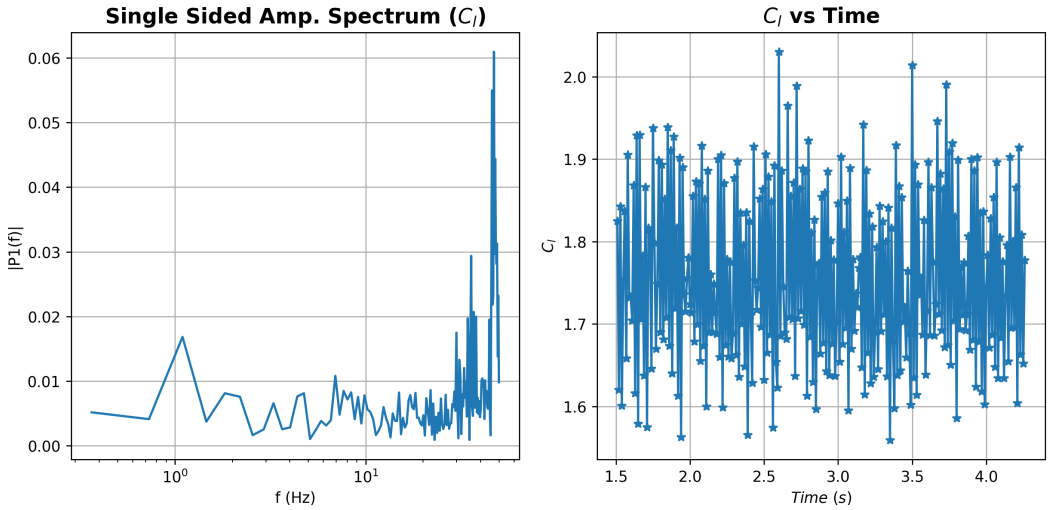

FIGURE 3.9: FFT for C_{lift}

As shown above, the Fast Fourier Transfer is applied to calculate the oscillation frequency at the angle of attack of 18.9 degrees. The direct results as well as the Strouhal number related to the max energy frequency are shown below in Table 3.2, from which the main model of the flow topology can be identified because the imaginary part of its eigenvalue is related to the Strouhal number as $w_i = 2\pi St$.

oscillation parameters	
oscillation amplitude	4.706e-01
frequency of max energy	47.08

parameters interested	
Strouhal Number	0.912
imaginary part of the eigenvalue	5.732

TABLE 3.2: FFT results

3.4 Stability analysis results

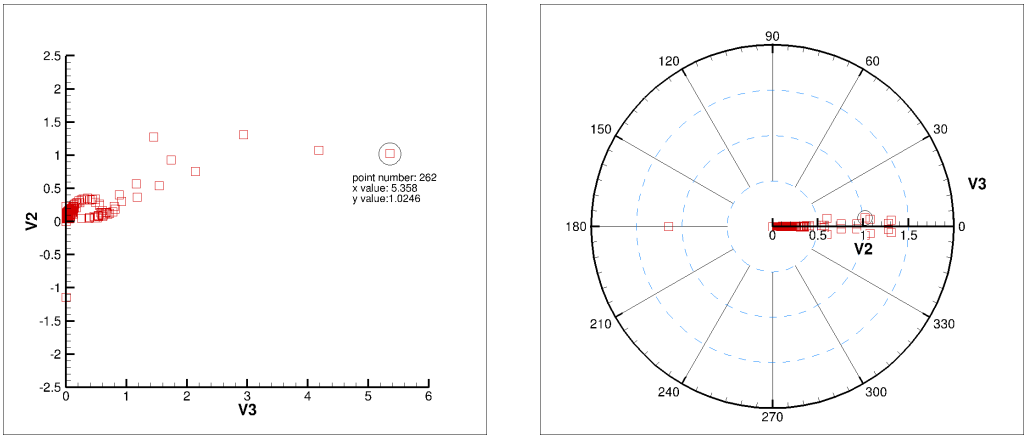

(A) x-z plot (B) polar plot

FIGURE 3.10: eigenvalue plots

The coordinates of the main eigenvalues are shown in Figure 3.10 above. The x-z map is the same as that in Chapter 2, in which the eigenvalue is determined to be unstable if the z coordinate exceeds zero. In the polar plot, the angle and radius are shifted from the x and z axes in the Cartesian coordinate. The eigenvalues of interest have radius coordinates greater than 1. After selecting and filtering the noise eigenvalues and reference the previous FFT results, the point marked on the figure is chosen and the related model is obtained as flows.

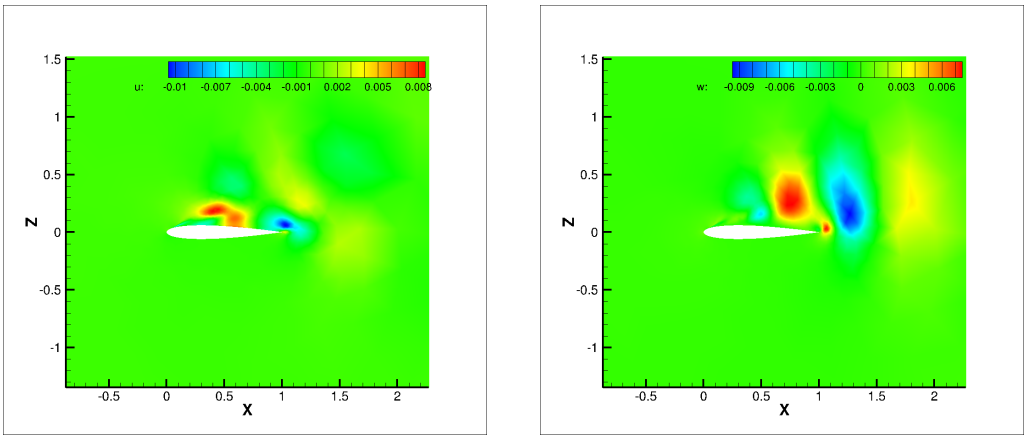

(A) v_X contour (B) v_z contour

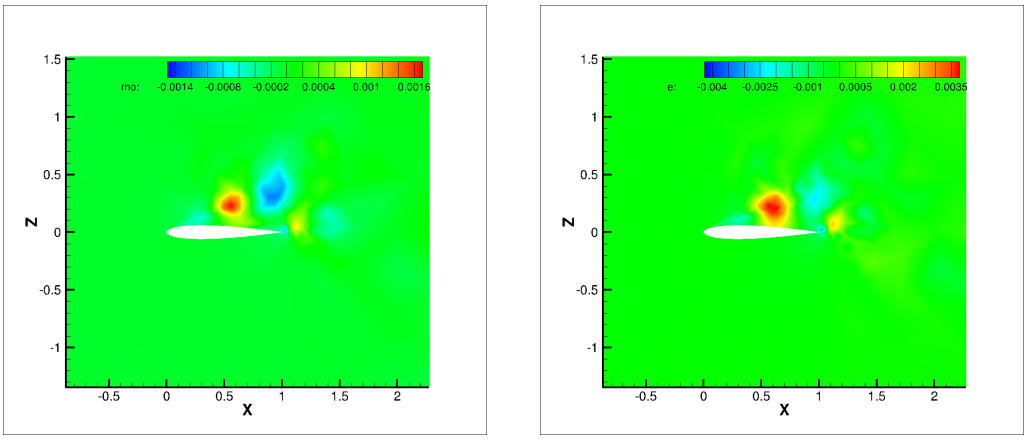

(A) density contour (B) gas energy contour

FIGURE 3.12: contours for unsteady model

3.5 Summary and conclusions

In this case, a set of simulation towards NACA0012 airfoil is performed with a quasi 3D structured mesh. First, steady flow simulation method is applied to calculate changes of C_{lift} and C_{drag} as a function of angle of attack, which meets well with the standard result.

After that, unsteady flow simulation is adopted to identify the critical angle of attack as 18.9 degrees of which the results are set as the object of stability analysis. Meanwhile, the FFT process is enacted obtaining the oscillation amplitude as 4.706e-01 and frequency of max energy as 47.08 HZ. With a calculation of Strouhal number as 0.912, the imaginary part of the eigenvalue ralated to the eigenmode with the maximum energy is obtained as $W_i = 5.732$. Finally, with stability analysis, the dominant model is extracted and visualised.

Chapter 4

Transonic injector case

4.1 Simulation setting

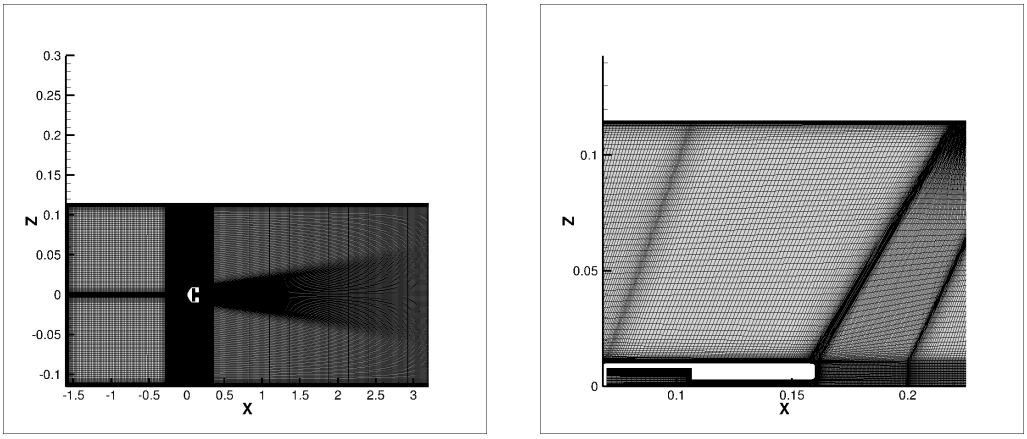

(A) overall view (B) detailed view

FIGURE 4.1: mesh used in straight trailing edge case

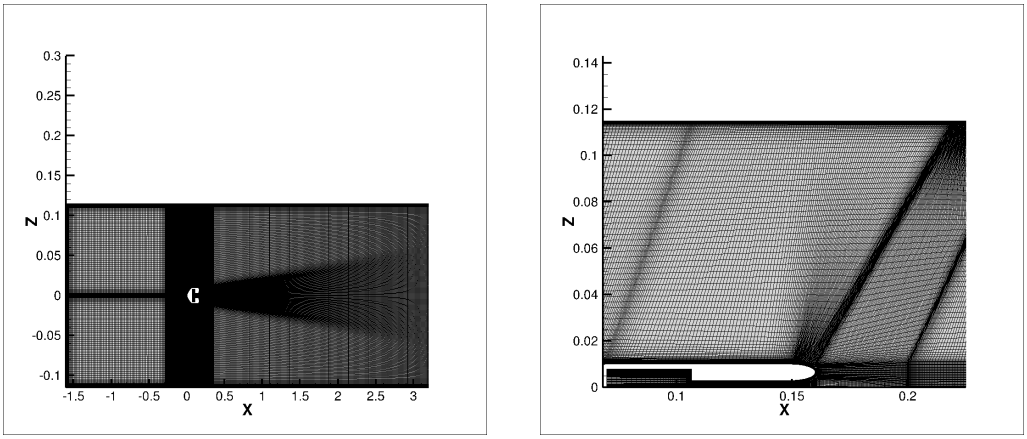

(A) overall view (B) detail view

FIGURE 4.2: mesh used in rounded trailing edge case

In this case, 2 kinds of injectors are compared with each other, the one with rectangular trailing edge tips, referred as straight trailing edges, and the one with elliptical trailing edge tips, known as rounded trailing edges. Similar quasi-three-dimensional structured grids with the former cases are applied, the overall and local topology for each case are shown above in Figure 4.1 and Figure 4.2. The computation domain is

set as a rectangular area in the x-z plane defined by points (-0.1,0,-1.5) and (0.1,0,3). The injector with the length of 0.15 is settled in the middle, whose leading edge coordinate is (0,0,0).

As for the parameters chosen in this case, the base flow is computed under the reference Mach number $Ma_r = 0.9$, with a Reynolds length number 0.16 considering the transonic condition. Other parameters are chosen according to the perfect gas assumption and standard atmosphere theory (shown in Table 4.1).

Perfect gas thermodynamic	
Gas constant R	287
Gas constant gamma	1.4
Transport coefficients	
Prandtl number	0.72
Sutherland constant	110.4

References	
Reynolds length	0.160
Reference Mach number	0.9
Reference pressure	101325
Reference temperature	391.62

TABLE 4.1: Parameters used in jetflow case

In either case, far filed boundary condition is applied at the external boundary of the domain and no-slip wall condition is enacted to the surface of the injector. Different from former chapters, a bleeding boundary condition is introduced purging into base region from the rear end of the injector with a bleeding coefficient $C_b = p_{purge}/p_0 = 0.7$. The computation is set as unsteady. And $k - \omega$ turbulence model is chosen in this flow regime. Detailed flow parameters of the two cases are attached in appendix A.3 and A.4.

Besides, it is worth to mention that both of the two cases are computed on the basis of a former result, set as restart file.

4.2 Simulation process

As illustrated in Figure 4.3 below, at first, unsteady simulations with the profiling process are both performed in two trailing edges cases. The base flow solution is compared with each other in the conclusion part of this section.

As in the straight case, the solution is set as outputting one result every 100 iterations. After the whole iterative process, the animation is composed of contours of x-velocity. As for the rounded case, instead of creating an animation, a profiling process at 14 points is conducted during the iteration and an FFT process is also performed onto the monitor data of x velocity.

Unfortunately, the expecting BiGlobal stability analysis fails because of a wrong solution of half mesh. According to previous work, which analyses the subsonic or supersonic condition, in order to identify the non-symmetric model on the injector case, the base flow should be computed with half of the mesh with an additional symmetric boundary layer on the axis of the injector. Because this process is able to create a symmetric steady base flow by mirroring the half-domain as a whole where the stability analysis will be completed. However in this transonic case, unfortunately, due to the complexity of the flow topology, this methodology failed. The results of the half-mesh domain do not match the solution of a full domain simulation.

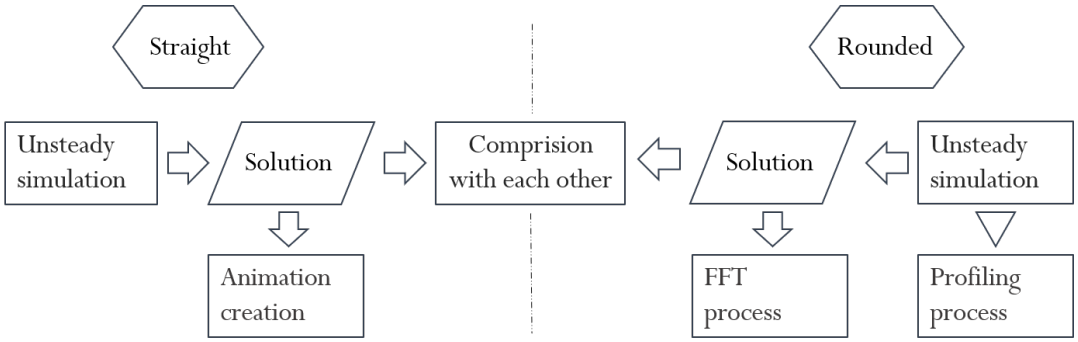

FIGURE 4.3: simulation process

4.3 Base flow results

4.3.1 Straight trailing edge injector

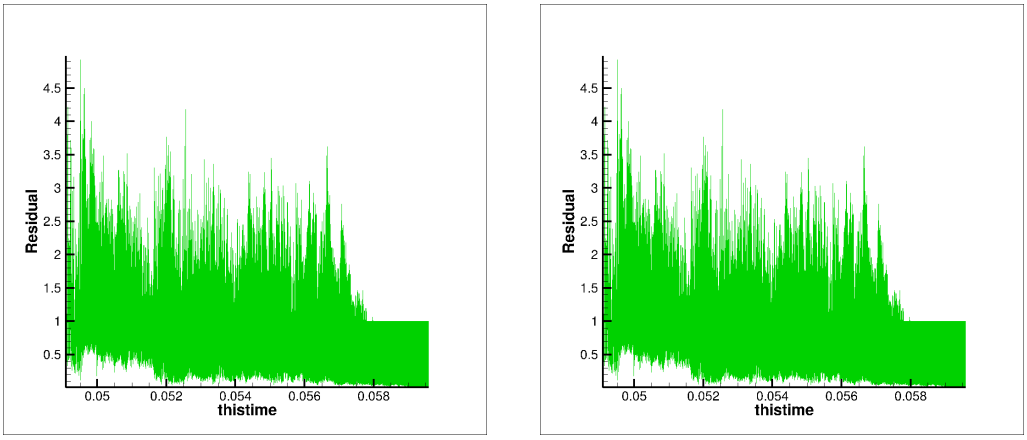

(A) overall view (B) detail view

FIGURE 4.4: residual monitor

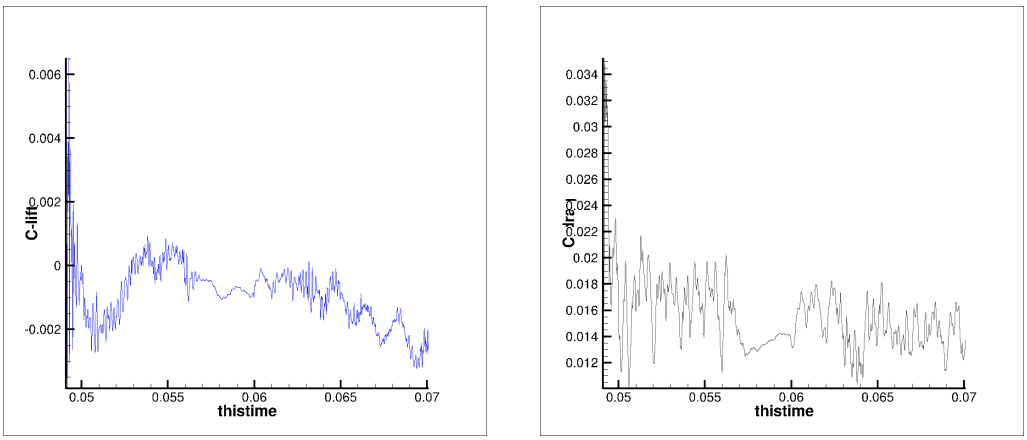

(A) C_{lift} monitor (B) C_{drag} monitor

FIGURE 4.5: C_{lift} & C_{drag} monitor

Figure 4.4 and 4.5 illustrate how the residual and the values of lift coefficient & drag coefficient change with the time step. As it is shown in Figure 4.4, after an irregular fluctuation period before 0.058s, a periodic oscillation pattern of residual appears. In the drag and lift plots, however, irregular oscillation occurs throughout the whole iteration process. A possible reason is proposed in the conclusion section after compared with the results of the rounded case.

Messy as it is from the perspective of C_lift and C_drag monitor data. The solutions of intermediate time steps, known as temporal snapshots, extracted afterwards, seem reasonable. Instead of showing the animation that generated, several internal step results are shown in Fig 4.6. below.

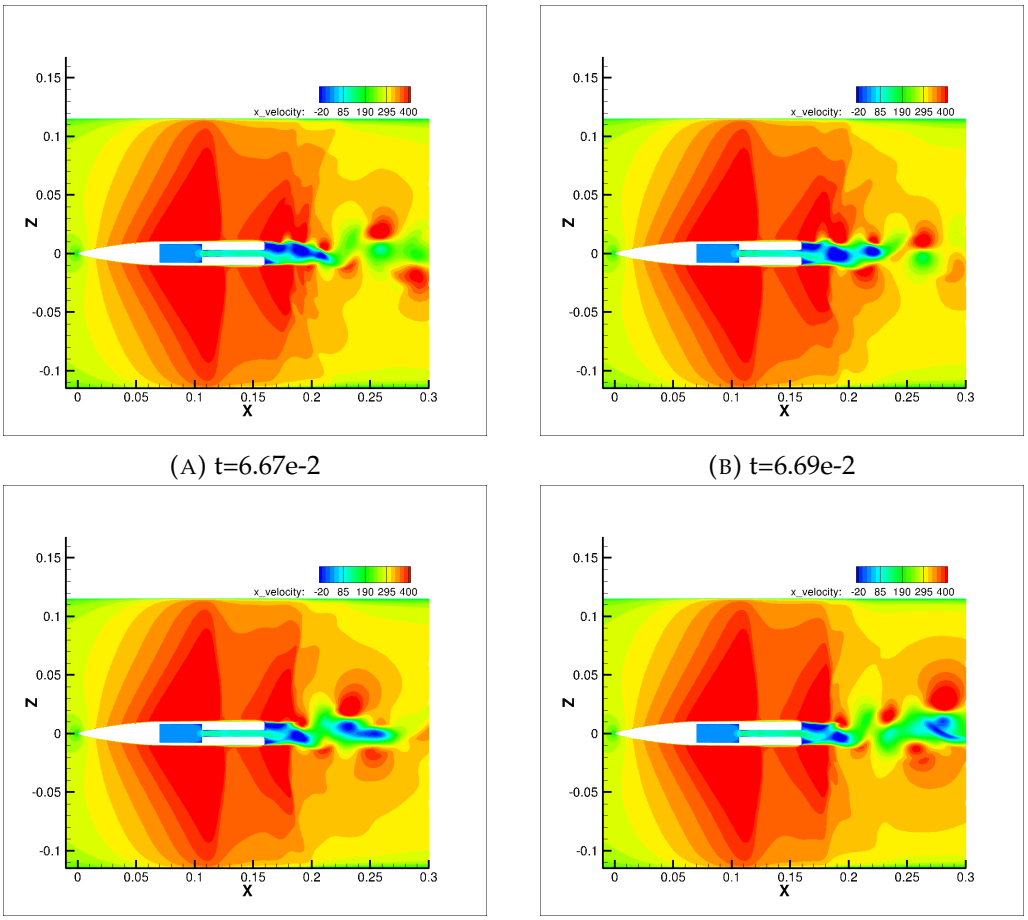

(A) t=6.67e-2 (B) t=6.69e-2

(C) t=6.73e-2 (D) t=6.75e-2

FIGURE 4.6: temporal snapshot of straight case

From the temporal snapshot of horizontal velocity contours, it is clear to see the flow accelerates and reaches the local sound velocity at the end the nose ogive and the rear end of the injector creating two sets of symmetric oblique shock waves. At the wake flow of the trailing edge, an asymmetric topology manifests clearly, with the vortex separating, breaking and shedding from the trailing edge with time.

4.3.2 Rounded trailing edge injector

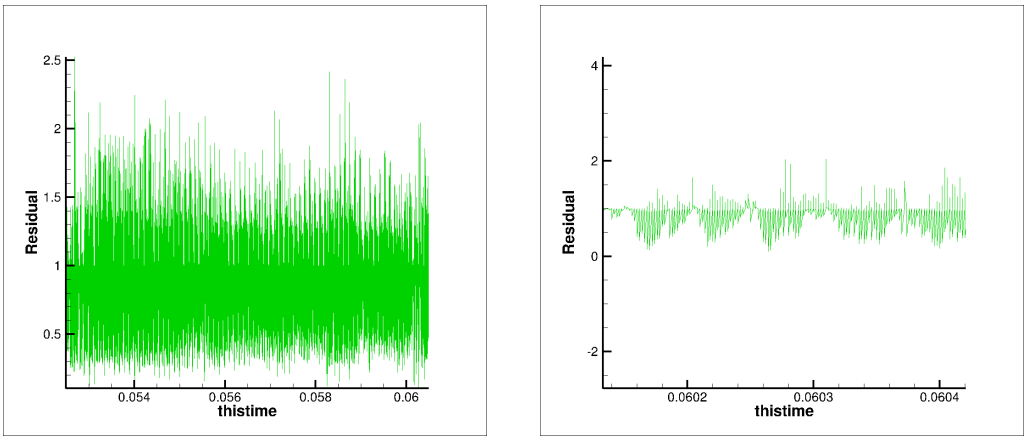

(A) overall view (B) detail view

FIGURE 4.7: residual monitor

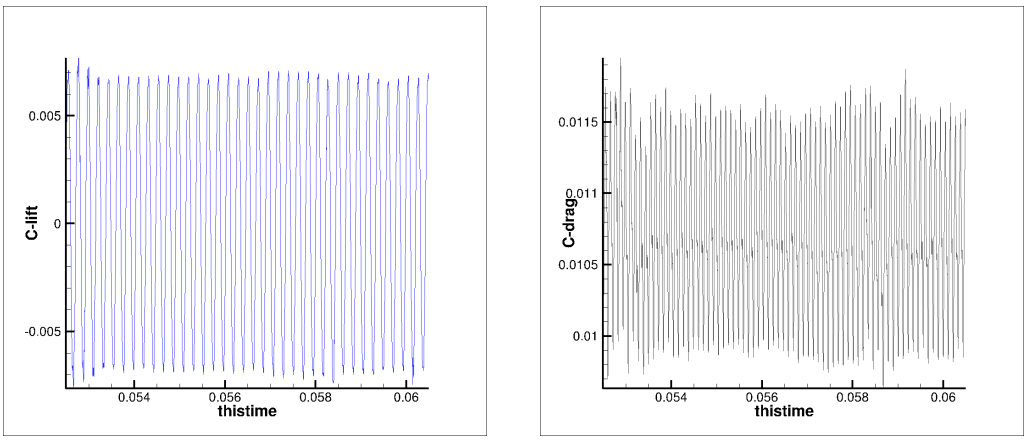

(A) C_{lift} monitor (B) C_{drag} monitor

FIGURE 4.8: C_{lift}&C_{drag} monitor

The behaviour of the residual and the values of lift coefficient & drag coefficient for the rounded trailing edge changing with the time step is shown in Figure 4.7 and Figure 4.8. Despite the seemingly irregular behaviour of residual, the results for C_{lift}&C_{drag} monitor in Figure 4.8 are quite satisfying as stable oscillation patterns happen to both of the flow variables. This can also be confirmed by the FFT result of the C_{lift} shown below in Figure 4.9.

Besides, the profiling processes (results are shown in Figure 4.10 and Figure 4.11) toward v_X and v_y were also done recording the velocity change with iteration. It also shows a regular oscillating pattern in spite of slight fluctuations compared to the average oscillation amplitude.

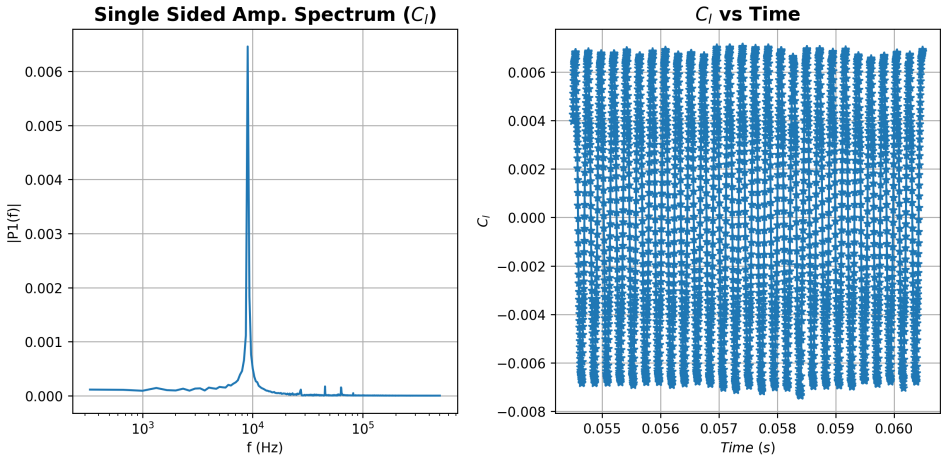

FIGURE 4.9: FFT results

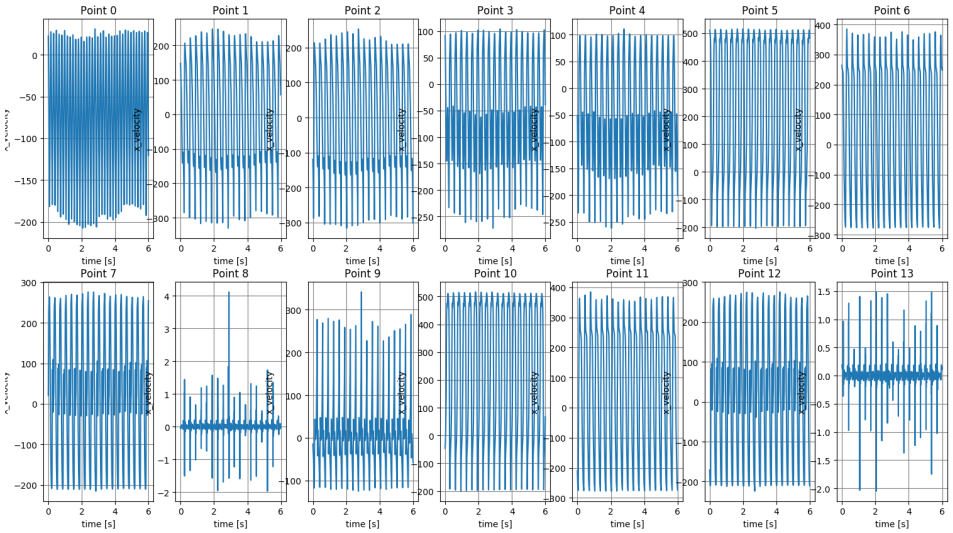

FIGURE 4.10: profiling results of x velocity

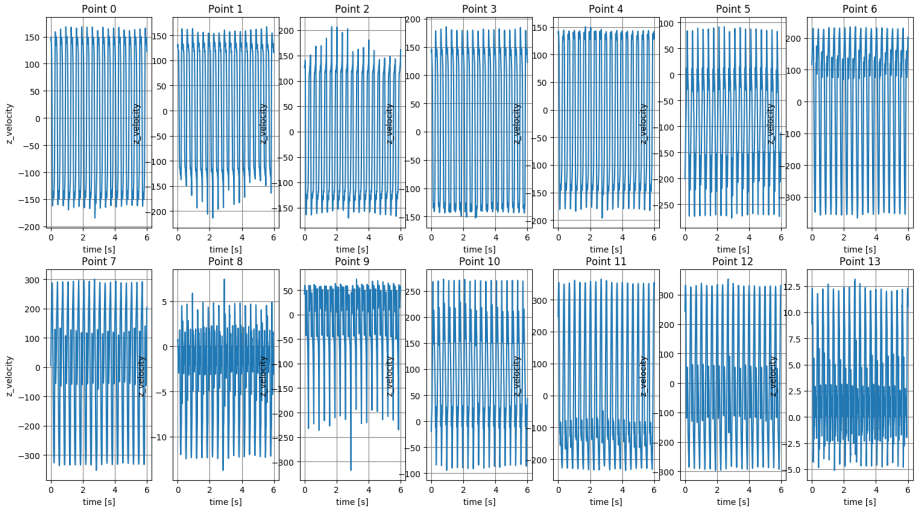

FIGURE 4.11: profiling results of y velocity

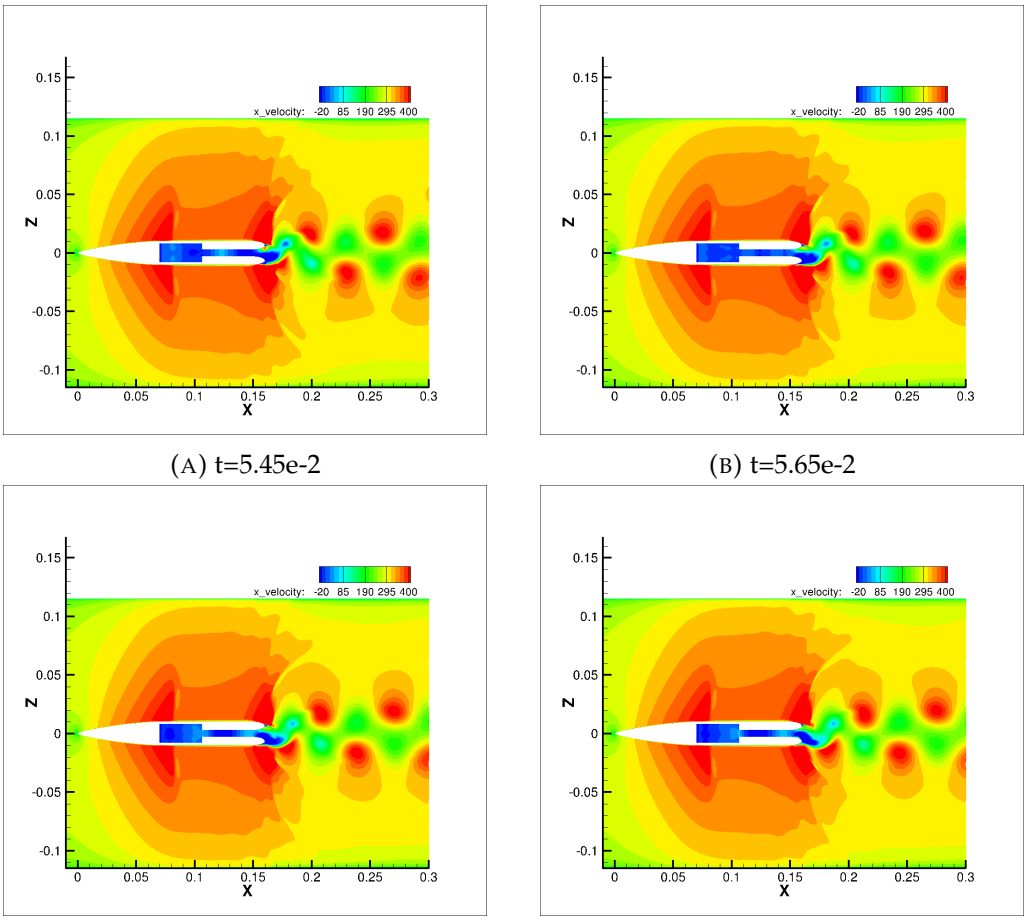

(A) t=5.45e-2 (B) t=5.65e-2

(C) t=5.85e-2 (D) t=6.05e-2

FIGURE 4.12: middle results in rounded case

The temporal snapshot of contours of velocity in the x-direction is shown above in Figure 4.12. From the figures, it is clear to see 2 sets of shock waves and vortex shedding from the end of the body. The bifurcation phenomenon also occurs in this case.

4.4 Summary and conclusions

All in all, the non-symmetric jet-flow topology is detected and visualised in both straight and rounded scenarios. Comparing the flow topology of the two conditions, the rounded trailing edge case shows a less intense oblique shock. Besides, the vibration of the jet flow from the rectangular trailing edge shows a more irregular pattern from the monitor data. Since the trailing edge is the only different variable between the two cases, it is concluded that it is the sharp body shape that lead to the unstable vibration.

Chapter 5

Conclusions and future work

5.1 Conclusions

In this thesis, the TAU tools are successfully proven to be valid through a validation case, and applied to 2 cases. Quasi 3D meshes are used in both cases and similar boundary layer is applied as well except the injector has an additional bleeding boundary condition. Unsteady conditions are both detected with the visualisation of flow topology but the stability analysis process has only performed successfully on the airfoil case. Main conclusions are shown as follows:

First, the results of TAU calculating the NACA0012 airfoil case with a Mach number of 0.15 and a Reynolds number of 600,000 are in well agreement with experimental results.

Second, the critical angle of separation of the airfoil is 18.9 degrees. And the frequency of the max energy of the oscillation is 47.8HZ.

Third, Stability analysis can extract main model of the airfoil case and analyse the flow separation flow stability by visualising the model.

Fourth, the jet flow will bifurcate when shooting out of the injector at a transonic condition.

5.2 Future work

There are two main problems in this case. First, Due to the limit of time and computation resource, the mesh used in airfoil case is not quite dense as the contour results has to set as continuous colour band. Second, the stability analysis failed to performed on the transonic injector.

In the future, more density mesh and the more simulation points will set to increase the accuracy of the solutions. And airfoil ought to be optimised with the analysis of the model. For the injector case, other process will be enacted to perform the stability analysis.

Appendix A

Parameters details

A.1 Parameters of cylinder case

A.2 Parameters of airfoil case

```
 ----------------------------------------------------
BOUNDARY MAPPING
----------------------------------------------------

                    Markers: 6
                       Type: symmetry plane
                       Name: SymmPlane1
   Write surface data (0/1): 0
block end
---------------------------
                    Markers: 8
                       Type: symmetry plane
                       Name: SymmPlane2
   Write surface data (0/1): 0
block end
---------------------------
                    Markers: 1
                       Type: viscous wall
                    Subtype: laminar
                       Name: Cylinder
       Monitor forces (0/1): 1
   Write surface data (0/1): 1
block end
---------------------------
                    Markers: 2,3,4,7
                       Type: farfield
                       Name: Farfield
       Angle alpha (degree): 0.0
   Write surface data (0/1): 0
block end
---------------------------

----------------------------------------------------
PARTITIONING
----------------------------------------------------
    Partitioning -----------------------------------: -
             Use parallel initial partitioner (0/1): 1
                    Number of primary grid domains: 6
                                 Number of domains: 6

----------------------------------------------------
PREPROCESSING
----------------------------------------------------
   Grid/Solution ----------------------------------: -
                         Boundary mapping filename: (thisfile)
                             Primary grid filename: ./MESH/doubled_2D.taumesh
                                       Grid prefix: ./dua/dualgrid
                               Output files prefix: ./sol/cylinder-full

   OUTPUT-------------------------------------------:-
                                      Output level: 10
   MULTIGRIDDING------------------------------------:-
                       Number of multigrid levels: 2
   ACCELERATORS-------------------------------------:-
                 2D offset vector (0 / x=1,y=2,z=3): 2
   Parameter --------------------------------------: -
             Cache-coloring (0/max_faces in color): 10000
                       Compute lusgs mapping (0/1): 1
                        Sharp edge angle (degrees): 0
                      Bandwidth optimisation (0/1): 0

----------------------------------------------------
SOLVER
----------------------------------------------------
     Timestepping Start/Stop ------------------------: -
                                      Output period: 199999
```

```
                              Maximal time step number: 40000
                                      Minimum residual: 1e-7

    Files/IO ----------------------------------------: -
                        Automatic parameter update (0/1): 1
                    Automatic parameter update mode (0/1): 0
                              Accumulate queue time (0/1): 1
                      Write pointdata dimensionless (0/1): 0
    Reference system of forces and moments (tau/ln9300): tau

      Memory management -------------------------------: -
                                  Increase memory (0/1): 1

      Geometry ----------------------------------------: -
                                           Grid scale: 1
                                 Reference relation area: 1
                     Reference length (pitching momentum): 1
              Reference length (rolling/yawing momentum): 1
                                    Origin coordinate x: 0.0
                                    Origin coordinate y: 0.0
                                    Origin coordinate z: 0.0

      Transport coefficients --------------------------: -
                                        Prandtl number: 0.72
                                   Sutherland constant: 110.4
      References --------------------------------------: -
                                       Reynolds length: 1.0
                                       Reynolds number: 60
                                  Reference Mach number: 0.2

      Universal ---------------------------------------: -
                                          Solver type: Flow
                               Viscous calculation (0/1): 1
      # Set 0 value for Euler flow calculation, and 1 for laminar&turbulent flows

      Monitoring --------------------------------------: -
                                  Monitor history (0/1): 1
                        Residual monitoring type (0/1): 1
                                    Monitoring values: Rrho_Max-Rrho_C-drag_C-
lift
                          Monitoring significant figures: 4_8_8_8_8
                     Extended coefficient monitoring (0/1): 1
           # Set to 1 to separate between pressure & viscous forces on output
monitor

      Flux main ---------------------------------------: -
                     Inviscid flux discretization type: Central
                      Viscous flux type TSL/Full (0/1): 1
                           Mixed inviscid fluxes (0/1): 0
      Central flux ------------------------------------: -
                             Central dissipation scheme: Scalar_dissipation
                      Central convective meanflow flux: Average_of_flux
                    Central convective turbulence flux: Average_of_flux
                      2nd order dissipation coefficient: 0.5
              Inverse 4th order dissipation coefficient: 64
                 Version of cell stretching coefficient: TAU
                  Use modified dissipation for 2D (0/1): 0

      Relaxation --------------------------------------: -
                                  Relaxation solver: Backward_Euler

      Multigrid ---------------------------------------: -
                              MG description filename: sg
                         SG start up steps (fine grid): 50
               Turbulence equations use multigrid (0/1): 0
```

```
     Timestepsize ------------------------------------: -
                                        CFL number: 20.0
                            CFL number (coarse grids): 20.0
                            CFL number (large grad p): 20.0

     Preconditioning ---------------------------------: -
                                     Preconditioning: (none)
                                       Cut-off value: 1

------------------------------------------------------
Non-steady calculations
------------------------------------------------------
     Dual time ---------------------------------------: -
                               Unsteady time stepping: dual
        Unsteady activate inner iteration output (0/1): 1
                 Unsteady show pseudo time steps (0/1): 1
                      Unsteady physical time step size: 0.003
                         Unsteady physical time steps: 4000
                Unsteady inner iterations per time step: 30
    Flow time averaging -----------------------------: -
                              Compute flow statistics: mean

------------------------------------------------------
Profile output parameters:
------------------------------------------------------
                       Profile output description file: (thisfile)
                                 Profile output period: 2000
                                 Profile every n steps: 1
                                 Profile output values: xyz_p_rho_v
                              Wall boundary point (0/1): 0
                                   Number of profiles: 11
 Profile support x: 1.0 1.0 1.0 1.0 1.0 1.0  1.0  1.0  1.0  1.0  1.0
 Profile support y: 0.0 0.0 0.0 0.0 0.0 0.0  0.0  0.0  0.0  0.0  0.0
 Profile support z: 0.5 0.4 0.3 0.2 0.1 0.0 -0.1 -0.2 -0.3 -0.4 -0.5
------------------------------------------------------
Analysis parameters:
------------------------------------------------------
                                        Analysis file: pfile
                                   Analysis request: profile
                             Analysis profile request: all
                                   Analysis variables: p_rho
                             Analysis inner loop (0/1): 0
                              Analysis averaging (0/1): 0
        Analysis write coordinates in grid units (0/1): 1
                           Analysis data format string: %-18.9e
                                Analysis output format: tecplot
                                Analysis output prefix: point
                         ## Needed in parallel computations!! ##
                          Extract nearest profile (0/1): 1


------------------------------------------------------
Extra field pointdata output
------------------------------------------------------
                         Field output description file: (thisfile)
                                   Field output values: mach_cp_vort

------------------------------------------------------
Surface output parameters:
------------------------------------------------------
                       Surface output description file: (thisfile)
                                 Surface output values: cp_xyz_cf_restart
                                 Surface output period: 1999999
```

```
-----------------------------------------------------
 BOUNDARY MAPPING
 -----------------------------------------------------

                     Markers: 3
                        Type: symmetry plane
                        Name: SymmPlane1
    Write surface data (0/1): 1
 block end
 ----------------------------
                     Markers: 4
                        Type: symmetry plane
                        Name: SymmPlane2
    Write surface data (0/1): 1
 block end
 ----------------------------
                     Markers: 1
                        Type: viscous wall
                     Subtype: turbulent
                        Name: Airfoil
     Use wall function (0/1): 0
        Monitor forces (0/1): 1
    Write surface data (0/1): 1
 block end
 ----------------------------
                     Markers: 2
                        Type: farfield
                        Name: Farfield

        Angle alpha (degree): 18
         Angle beta (degree): 0.0

     Vortex correction (0/1): 0
                 Chord length: 1.0

    Write surface data (0/1): 1
 block end
-------------------------

 -----------------------------------------------------
 PARTITIONING
 -----------------------------------------------------
     Partitioning -----------------------------------: -
                 Use parallel initial partitioner (0/1): 1
                         Number of primary grid domains: 16
                                      Number of domains: 16

 -----------------------------------------------------
 PREPROCESSING
 -----------------------------------------------------
    Grid/Solution ----------------------------------: -
                             Boundary mapping filename: (thisfile)
                                 Primary grid filename: ./MESH/J1.grid
                                           Grid prefix: ./dua/dual_NACA0012
                                 Output files prefix: ./sol/NACA0012lam

    OUTPUT-------------------------------------------:-
                                        Output level: 99
    MULTIGRIDDING------------------------------------:-
                           Number of multigrid levels: 3
    ACCELERATORS-------------------------------------:-
                      2D offset vector (0 / x=1,y=2,z=3): 2
    Parameter ----------------------------------------: -
                 Cache-coloring (0/max_faces in color): 10000
                           Compute lusgs mapping (0/1): 1
                            Sharp edge angle (degrees): 0
```

```
                        Bandwidth optimisation (0/1): 0

 ------------------------------------------------------
 SOLVER
 ------------------------------------------------------
      Timestepping Start/Stop -------------------------: -
                                       Output period: 1999999
                                Maximal time step number: 20000
                                        Minimum residual: 1e-8

    Files/IO ----------------------------------------: -
                         Automatic parameter update (0/1): 1
                    Automatic parameter update mode (0/1): 0
                              Accumulate queue time (0/1): 1
                                           Output level: 10
                      Write pointdata dimensionless (0/1): 1
    Reference system of forces and moments (tau/ln9300): tau

      Memory management -------------------------------: -
                                  Increase memory (0/1): 1

      Geometry ----------------------------------------: -
                                        Grid scale: 1
                                 Reference relation area: 1
                   Reference length (pitching momentum): 1
             Reference length (rolling/yawing momentum): 1
                                  Origin coordinate x: 0.25
                                  Origin coordinate y: 0
                                  Origin coordinate z: 0

      Perfect gas thermodynamic -----------------------: -
                                       Gas constant R: 287
                                   Gas constant gamma: 1.4
      Transport coefficients --------------------------: -
                                       Prandtl number: 0.72
                                   Sutherland constant: 110.4
                         Sutherland reference viscosity: 1.7894e-05
                       Sutherland reference temperature: 288.15
      References --------------------------------------: -
                                     Reynolds length: 1.0
                                     Reynolds number: 6e6
                                 Reference Mach number: 0.15
      Variables ---------------------------------------: -
                             Fix negative values (0/1): 0
                                       Minimal density: 1e-12
                                      Minimal pressure: 1e-12
                                        Minimal energy: 1e-12

      Internal flow -----------------------------------: -
                               Init total conditions (0/1): 0

      Universal ---------------------------------------: -
                                        Solver type: Flow
                                    Viscous calculation (0/1): 1
      # Set 0 value for Euler flow calculation, and 1 for laminar&turbulent flows

      Monitoring --------------------------------------: -
                                  Monitor history (0/1): 1
                        Residual monitoring type (0/1): 1
                                     Monitoring values: Residual_C-drag_C-lift_C-
my_Max-res
                             Monitoring significant figures: 4_8_8_8_8
                    Extended coefficient monitoring (0/1): 0
                    # Set to 1 to separate between pressure & viscous forces on
output monitor
```

```
      Flux main ---------------------------------------: -
                     Inviscid flux discretization type: Central
                      Viscous flux type TSL/Full (0/1): 1
                           Mixed inviscid fluxes (0/1): 0
      Central flux ------------------------------------: -
                            Central dissipation scheme: Scalar_dissipation
                       Central convective meanflow flux: Average_of_flux
                     Central convective turbulence flux: Average_of_flux
                       2nd order dissipation coefficient: 0.5
              Inverse 4th order dissipation coefficient: 64
                 Version of cell stretching coefficient: TAU
                  Use modified dissipation for 2D (0/1): 0

     Gradients  --------------------------------------: -
                   #        Reconstruction of gradients: Least_square
                            Reconstruction of gradients: Green_Gauss

      Relaxation --------------------------------------: -
                                     Relaxation solver: Backward_Euler
                       Hold static velocity field (0/1): 0
      Backward Euler ----------------------------------: -
                                        Linear solver: Lusgs
                          Implicit overrelaxation omega: 1
                           Implicit overrelaxation beta: 1
      LUSGS -------------------------------------------: -
                                   Sgs stages maximum: 3
           Lusgs increased parallel communication (0/1): 0
                     Lusgs treat whirl implicitly (0/1): 0

      Multigrid ---------------------------------------: -
                               MG description filename: sg
                             Multigrid indicator (0/1): 0
                          SG start up steps (fine grid): 50
                Turbulence equations use multigrid (0/1): 0
           Coarse grid viscous flux type TSL/Full (0/1): 0
      Full multigrid ----------------------------------: -
                                Multigrid start level: 1
                 Maximal time step number (coarse grids): 100
                          Minimum residual (coarse grids): 0.001
        Full multigrid central scheme first-order (0/1): 1

      Timestepsize ------------------------------------: -
                                          CFL number:
200000000000000000000000000.0
                               CFL number (coarse grids):
200000000000000000000000000.0
                               CFL number (large grad p):
200000000000000000000000000.0
                              Time step smoothing factor: 0
      Smoother ----------------------------------------: -
                                    Residual smoother: Point_explicit
                                  Correction smoother: Point_explicit
                               Correction smooth epsilon: 0.2
                                 Residual smooth epsilon: 0.2002
                               Correction smoothing steps: 2
                                 Residual smoothing steps: 2
      Preconditioning ---------------------------------: -
                                       Preconditioning: (none)
                                         Cut-off value: 1

      Turbulence --------------------------------------: -
                                       Turbulence mode: RANS
                                 Turbulence model version: SA
                                        SA model version: SAO
                                   Ratio Prandtl lam/turb: 0.8
                                General ratio mue-t/mue-l: 0.1
```

```
                            Maximum limit mue-t/mue-l: 20000
                          General turbulent intensity: 0.001
                               Reference bl-thickness: 1e+22
                                    Positivity scheme: 0
                                EARSM expansion order: 1
                        Vortical flow correction (0/1): 0
          Turbulence diffusion flux type TSL/Full (0/1): 1
     SA models ----------------------------------------: -
                             SA boundary condition type: smooth
                     SA attractor for zero value (0/1): 0
                   SA mixing compress correction (0/1): 0

 ------------------------------------------------------
 Non-steady calculations
 ------------------------------------------------------
     Dual time ----------------------------------------: -
                                Unsteady time stepping: (none)
        Unsteady activate inner iteration output (0/1): 1
                  Unsteady show pseudo time steps (0/1): 1
                       Unsteady physical time step size: -1
                          Unsteady physical time offset: 0
                  Unsteady computational time step size: 0.1
                            Unsteady physical time steps: 4000
                Unsteady inner iterations per time step: 1000
      Minimum number of inner iterations per time step: 0
                          Unsteady implicit scheme order: 2
                            Unsteady extrapolation order: 1
           Compute harmonics of global forces (0/1..n): 0
                     Compute harmonics on surface (0/1): 0
     Moving grid --------------------------------------: -
                                  Type of grid movement: static
                             Motion description filename: (none)
                               Motion hierarchy filename: (none)
                         Extended motion monitoring (0/1): 0
                         Geometric conservation law (0/1): 1
                             Initialize deformation (0/1): 0
    Flow time averaging -----------------------------: -
                                Compute flow statistics: (none)
            #          Reinitialize flow averaging (0/1): 0

 ------------------------------------------------------
 Extra field pointdata output
 ------------------------------------------------------
                                                        Field output description file:
(thisfile)
                                                        Field output values: mach

 ------------------------------------------------------
 Surface output parameters:
 ------------------------------------------------------
                        Surface output description file: (thisfile)
                                  Surface output values: imach
                                  Surface output period: 1999999



    solver at Mon May  6 18:57:30 2019
                                  Restart-data prefix: ./sol/NACA0012lam.pval.20000
                         SG start up steps (fine grid): 0
    solver at Mon May  6 18:57:30 2019
                                   Surface output filename: ./sol/
NACA0012lam.surface.pval.20000
    solver at Mon May  6 20:54:58 2019
                                  Restart-data prefix: ./sol/NACA0012lam.pval.
40000
    solver at Mon May  6 20:54:58 2019
```

Acknowledgements

Thanks to Professor Eusebio Valero and Vice professor Yaguo Lyu for their careful guidance on the graduation project. Thanks to Yinzhu Wang for guiding me on the subject, linux system. Thanks to Martinez-Cava Alex for support for the TAU, TAUev software. And thanks to Binghua LI for technical support for the college server Bender.

Thanks to my parents, my roommates and all my friends for their support, who have been encouraging me behind me and promoting me. They are my greatest spiritual support. Thanks to the funded support from the "Erasmus+ scholarship" of the European Commission. Plus thanks to the teachers of the Escuela Técnica Superior de Ingeniería Aeronáutica y del Espacio, the Foreign Affairs Offices of Northwestern Polytechnical University and Universidad Polétechica de Madrid and teachers from School of Power and Energy for their help.

At last, I would like to thank all the people who helped me during the graduation project!

Bibliography

[1] Osborne Reynolds. Xxix. an experimental investigation of the circumstances which determine whether the motion of water shall be direct or sinuous, and of the law of resistance in parallel channels. *Philosophical Transactions of the Royal society of London*, (174):935–982, 1883.

[2] Mårten T Landahl, Eric Mollo-Christensen, and Murray S Korman. Turbulence and random processes in fluid mechanics, 1989.

[3] CC Kin. *The theory of hydrodynamic stability*. Cambridge University Press, Cambridge, 1955.

[4] PG Drazin and LN Howard. Hydrodynamic stability of parallel flow of inviscid fluid. In *Advances in applied mechanics*, volume 9, pages 1–89. Elsevier, 1966.

[5] Patrick Huerre and Peter A Monkewitz. Local and global instabilities in spatially developing flows. *Annual review of fluid mechanics*, 22(1):473–537, 1990.

[6] S Scott Collis, Ronald D Joslin, Avi Seifert, and Vassilis Theofilis. Issues in active flow control: theory, control, simulation, and experiment. *Progress in aerospace sciences*, 40(4-5):237–289, 2004.

[7] RT Pierrehumbert and SE Widnall. The two-and three-dimensional instabilities of a spatially periodic shear layer. *Journal of Fluid Mechanics*, 114:59–82, 1982.

[8] Vassilios Theofilis. Advances in global linear instability analysis of nonparallel and three-dimensional flows. *Progress in aerospace sciences*, 39(4):249–315, 2003.

[9] Vassilios Theofilis. Global linear instability. *Annual Review of Fluid Mechanics*, 43:319–352, 2011.

[10] JM Luijkx and JK Platten. On the onset of free convection in a rectangular channel. *Journal of Non-Equilibrium Thermodynamics*, 6(3):141–158, 1981.

[11] CP Jackson. A finite-element study of the onset of vortex shedding in flow past variously shaped bodies. *Journal of fluid Mechanics*, 182:23–45, 1987.

[12] A Zebib. Stability of viscous flow past a circular cylinder. *Journal of Engineering Mathematics*, 21(2):155–165, 1987.

[13] M Morzynski and F Thiele. Numerical stability analysis of a flow about a cylinder. *Zeitschrift Angewandte Mathematik und Mechanik*, 71:T424–T428, 1991.

[14] Alexander Yu Gelfgat. Different modes of rayleigh–bénard instability in two- and three-dimensional rectangular enclosures. *Journal of Computational Physics*, 156(2):300–324, 1999.

[15] Vassili Kitsios, Laurent Cordier, J-P Bonnet, Andrew Ooi, and Julio Soria. On the coherent structures and stability properties of a leading-edge separated aerofoil with turbulent recirculation. *Journal of Fluid Mechanics*, 683:395–416, 2011.

[16] A Tuck and J Soria. Separation control on a naca 0015 airfoil using a 2d micro znmf jet. *Aircraft Engineering and Aerospace Technology*, 80(2):175–180, 2008.

[17] V Theofilis, D Barkley, and S Sherwin. Spectral/hp element technology for global flow instability and control. *The Aeronautical Journal*, 106(1065):619–625, 2002.

[18] Rafael S Gioria, Wei He, and Vassilis Theofilis. On global linear instability mechanisms of flow around airfoils at low reynolds number and high angle of attack. *Procedia IUTAM*, 14:88–95, 2015.

[19] Daniel Rodríguez and Vassilis Theofilis. On the birth of stall cells on airfoils. *Theoretical and Computational Fluid Dynamics*, 25(1-4):105–117, 2011.

[20] C Wales, A Gaitonde, and D Jones. An initial study of the flow around an aerofoil at high reynolds numbers using continuation. *International Journal of Bifurcation and Chaos*, 22(10):1250255, 2012.

[21] C Wales, AL Gaitonde, and DP Jones. Continuation methods applied to the 2d navier–stokes equations at high reynolds numbers. *International Journal for Numerical Methods in Fluids*, 70(10):1258–1289, 2012.

[22] Yangang Wang and Longbo Zhao. Investigation on the effect of trailing edge ejection on a turbine cascade. *Applied Mathematical Modelling*, 37(9):6254–6265, 2013.

[23] M Raffel and F Kost. Investigation of aerodynamic effects of coolant ejection at the trailing edge of a turbine blade model by piv and pressure measurements. *Experiments in Fluids*, 24(5-6):447–461, 1998.

[24] FH KostI and AT Holmes. Aerodynamic efpect ov coolant ejection in the rear part of transonic rotor blades. *Best Available*, 1985.

[25] Dieter E Bohn, Volker J Becker, Klaus D Behnke, and Bernhard F Bonhoff. Experimental and numerical investigations of the aerodynamical effects of coolant injection through the trailing edge of a guide vane. In *ASME 1995 International Gas Turbine and Aeroengine Congress and Exposition*, pages V004T09A026–V004T09A026. American Society of Mechanical Engineers, 1995.

[26] BH Saracoglu, G Paniagua, S Salvadori, F Tomasoni, S Duni, T Yasa, and A Miranda. Trailing edge shock modulation by pulsating coolant ejection. *Applied Thermal Engineering*, 48:1–10, 2012.

[27] John David Anderson Jr. *Fundamentals of aerodynamics*. Tata McGraw-Hill Education, 2010.

[28] & Barakos G. N. Lawson, S. J. Review of numerical simulations for high-speed, turbulent cavity flows. *Progress in Aerospace Sciences*, 47(3):186–216, 2011.

[29] W. Rodi. Comparison of les and rans calculations of the flow around bluff bodies. *J.wind Eng.ind.aerodyn*, 69-71(none):55–75, 1997.

[30] R. J. Leveque. Finite volume methods for hyperbolic problems. *Meccanica*, 39(1):88–89, 2004.

[31] W. Kyle Anderson, James L. Thomas, and Bram Van Leer. Comparison of finite volume flux vector splittings for the euler equations. *Aiaa Journal*, 24(9):1453–1460, 2015.

[32] W. E Arnoldi. The principle of minimized iterations in the solution of the matrix eigenvalue problem. *Quarterly of Applied Mathematics*, 9(1):17–29, 1951.

[33] Y. Saad. Variations on arnoldi's method for computing eigenelements of large unsymmetric matrices. *Linear Algebra & Its Applications*, 34(1):269–295, 1980.

[34] C H K Williamson. Vortex dynamics in the cylinder wake. *Annual Review of Fluid Mechanics*, 28(1):477–539, 2003.

[35] Dwight Barkley and Ronald D. Henderson. Three-dimensional floquet stability analysis of the wake of a circular cylinder. *Journal of Fluid Mechanics*, 322(322):215–241, 1996.

[36] Langley Research Center. 2d naca0012 airfoil validation case, 2018.